Kinked and forked crack arrays in anisotropic elastic bimaterials

Aurélien Vattre

Kinked and forked crack arrays in anisotropic elastic bimaterials

A. Vattré[a,*]

[a] *Université Paris-Saclay, ONERA, Matériaux et Structures, 92322, Châtillon, France*

Abstract

The fracture problem of multiple branched crack arrays in anisotropic bimaterials is formulated by use of the Stroh formalism to the linear elasticity theory of dislocations. The general full-field solutions are obtained from the standard technique of distributed dislocations along finite-sized cracks of arbitrary shapes, which are embedded in dissimilar anisotropic half-spaces under far-field stress loading conditions. The bimaterial boundary-value problem leads to a set of coupled integral equations of Cauchy-type that is numerically solved by using the Gauss-Chebyshev quadrature scheme with appropriate boundary conditions for kinked and forked crack arrays. The path-independent J_k-integrals as crack propagation criterion are therefore evaluated for equally-spaced cracks, while the limiting configuration of individual cracks is theoretically described by means of explicit expressions of the local stress intensity factors $\boldsymbol{K}$ for validation and comparison purposes on several crack geometries. The short-range interactions resulting from the idealized configurations of infinitely periodic cracks are investigated as well as various size- and heterogeneity- effects on the mixed-mode cracks in complex stress-state environments. The influences of anisotropic elasticity, elastic mismatch, applied stress direction, inter-crack spacings and crack length ratios on the predictions from the J_k- and $\boldsymbol{K}$-based fracture criteria are examined in the light of different configurations from the single kinked crack case in a homogeneous medium to the network of closely-spaced forked cracks in presence of bimaterial interfaces.

Keywords: Continuous distributions of dislocations, anisotropic elasticity theory, heterogeneity, crack arrays, kinked and branched cracks, mixed-mode configurations

1. Introduction

The problem of cracks and fracture mechanics is an important wide-ranging research field of engineering science and mathematical physics since the pioneering theory developed by Griffith (1921), which forms the foundation of the modern continuum fracture mechanics. The cracks of various types and scales are found in many manufactured components, while their effects on the mechanical strength of solids are of continued concern. In many problems, failures and progressive damages are often related to interactions of multiple cracks in brittle or quasi-brittle materials such as concrete, rocks, ceramics and interface-dominated composite materials in bonded structures. In particular, the interaction effect among cracks has received considerable attention in the past decades, mainly because the disastrous failure events are preceded by the interaction and coalescence of those cracks. The theoretical analysis of the energetically favorable conditions for branched cracks to merge is therefore of importance in assessing structural integrity in many situations, including stress corrosion cracking, corrosion fatigue and thermal fatigue. The present work is part of the long-standing problems in fracture mechanics, namely 1) the determination of the stress fields produced by an infinite array of finite-length kinked and forked cracks of arbitrary geometry in anisotropic bimaterials, as well as 2) the corresponding configurational driving forces acting at the crack singularities. The bimaterials are subjected to arbitrary far-field stress state, and the arrays of branched cracks are represented as suitable continuous distributions of regularly-spaced dislocations, which are determined by a Cauchy-type singular integral equation and solved using series of Chebyshev polynomials. The isolated straight crack in an isotropic and homogeneous elastic medium is therefore a special limiting case, and is considered for validation purposes.

In many fracture mechanics problems in infinite isotropic solids, a large class of analytical solutions under plane stress and strain conditions in two dimensions is based on the fundamental work of complex potentials of Muskhelishvili (1953). This mathematical theory of plane elasticity has been used to treat the finite-length branched cracks (Chatterjee, 1975, Kitagawa et al., 1975, Lo, 1978) as well as the doubly-periodic array of straight cracks in an infinite isotropic medium (Fil'shtinskii, 1974, Ioakimidis and Theocaris, 1978, Panasyuk et al., 1977), within which the complex potential functions are taken as the unknown functions, and the Cauchy-type singular integral equations are established by obtaining these functions subjected to appropriate boundary conditions. For most of these solutions, the analysis is such that the limit for infinitesimally small kinks cannot be obtained readily from the analysis for finite kinks, leading to asymptotic expansions for stress intensity factors at the tips of infinitesimally small kinks (Amestoy and Leblond, 1992, Bilby and Cardew, 1975, Cotterell and Rice, 1980, Lo, 1978, Wu, 1978). Due to mathematical difficulties in many complicated branched-crack situations under non-uniform loading conditions, however, the Muskhelishvili complex potentials can not be readily applicable, while the alternative dislocation-based formalism (Bilby and Eshelby, 1968, Delameter et al., 1975, Stroh, 1958) can be used for more practical boundary value problems of structural materials containing branched cracks.

*Email address: aurelien.vattre@onera.fr

Dislocations and the corresponding elasticity of extrinsic and intrinsic dislocations are introduced into the theory of fracture mechanics in two directions. First, the nucleation and plastic flow of dislocations from the stressed crack tips are of great importance to determine the growth resistance of ductile metals (Kelly et al., 1967, Rice and Thomson, 1974), exhibiting the physical competition between Griffith cleavage and dislocation-mediated plastic shear at crack tips. Secondly, planar dislocations are viewed as mathematical elements to describe the displacement discontinuities along faults within the Earth's crust (Chinnery and Petrak, 1967, Weertman, 1964), semicoherent interfaces (Bilby et al., 1955, Bullough and Bilby, 1956, Vattré and Demkowicz, 2013) as well as crack surfaces (Bilby and Eshelby, 1968, Bilby and Cardew, 1975, Weertman, 1964) in classical elasticity theory. From the crystallographical picture, the crack plane dislocations of a mode I crack are climb edge dislocations, while the glide edge dislocations and screw dislocations are related to the mode II and III cracks, respectively. In practice, a complex crack problem leads also to a combinaison of continuum distribution of infinitesimal edge- and screw-type dislocations, such that the proper stress field produced by the cracks are calculated as a convolution of the multiple stress fields of dislocations with unknown distribution functions of dislocation densities. These densities are determined by satisfying the crack surface traction-free conditions, while the mixed-mode stress intensity factors are then written with respect to the local dislocation densities (Hills et al., 1996).

Since the seminal work of Volterra (1907) that lays out the theory of dislocation fields generated by a discontinuity of displacement in linear elastic bodies, much attention has been paid to the determination of the elastic interaction between single arbitrary-oriented dislocations and traction-free surfaces or internal interfaces, which is one the most important part of the elasticity theory of dislocations (Hirth and Lothe, 1992). Extensions of the single dislocation problems to periodic arrays of equally-spaced extrinsic and intrinsic dislocations have been addressed in both isotropic (Chou and Lin, 1975, Grekov and Sergeeva, 2020, Gutkin et al., 1989, Lubarda, 1997) and anisotropic (Chou, 1975, Chu and Pan, 2014, Gosling and Willis, 1994, Vattré and Pan, 2018) bimaterial solids, and this is the latter that is explored in the present two-dimensional analysis. Although the numerous discrete dislocation dynamics codes in the current literature are capable of exploring the collective evolution of random-oriented forest dislocations, lattice- and nodal-based simulations are essentially resorted to using the isotropic elastic solutions. In comparison with results from the full anisotropic elasticity, the elastic field solutions for dislocations (Asaro et al., 1973), the corresponding elastic energy and driving forces (Aubry et al., 2011, Barnett and Swasger, 1971), the reactions between glide dislocations and forest dislocations (Püschl, 1985) as well as the local relaxations between coplanar dislocations (Vattré, 2017a,b) can be altered by the isotropic elastic approximation. These significant consequences on the fundamental behavior of such elementary defects in solids suggest unequivocally that similar important effects due to elastic anisotropy are also prevalent and transferable in fracture mechanics.

In dislocation mechanics, the analysis of periodic dislocation arrays is of importance in modeling grain boundaries and heterophase interfaces as well as in understanding persistent slip bands that have dislocation cell structures. On the other hand, examination of periodic arrays of cracks is important in investigating the fracture processes of crack accumulation and coalescence (Kachanov, 1987, 2003), specially with specific collinear and straight cracks, for which the solutions based on the Muskhelishvili theory have been obtained by Koiter (1959), and more recently, in predicting the propagation of segmented crack fronts in mode I+III fracture (Lazarus et al., 2020, Leblond et al., 2014, 2015). The crack front segmentation in mixed mode I+III and I+II+III is therefore an illustrative example, for which the crack kinking and forking processes cannot be ignored when understanding the experimental crack front profiles and trajectories. Changes in crack path are generally induced by multi-axial stresses and/or the presence of microstructural inhomogeneities close to the crack tips, which can have a beneficial effect in the sense that crack kinking and forking improve the fracture toughness as well as the resistance to crack growth (Suresh and Shih, 1986). Furthermore, non-straight cracks with zig-zag growth of crack and the crack branching are also often be found in materials subjected to stress corrosion cracking and corrosion fatigue under mixed-mode loading conditions (Kitagawa et al., 1975). Such features have motivated and still motivate the development of various failure stress- and energy-based criteria for predicting the direction of crack propagation (Amestoy and Leblond, 1992, Azhdari and Nemat-Nasser, 1996, Cotterell and Rice, 1980, Erdogan and Sih, 1963, Gao and Chiu, 1992, Goldstein and Salganik, 1974, Ichikawa and Tanaka, 1982, Leguillon, 2002, Leguillon and Murer, 2008, Lin et al., 2010, Sih, 1974), importantly designed to investigate the configurational bifurcation and stability of cracks loaded under mixed-mode conditions.

By use of the linear elasticity theory of dislocations, a general singular integral equation formalism for two-dimensional fracture analysis of equally-spaced configurations of multiple branched cracks in bimaterials is proposed. The bimaterials are composed of two dissimilar orthotropic half-spaces under arbitrary far-field stress loading conditions. The content of the paper is organized as follows. Section 2 describes the boundary-value problem, within which the continuously distributed dislocations along the crack segments lead to a set of coupled integral equations of Cauchy-type that is numerically solved by the Gauss-Chebyshev quadrature scheme with appropriate boundary conditions for kinked and forked cracks. The full-field solutions are therefore used to evaluate the path-independent J_k-integrals as crack propagation criterion. The limiting case of individual cracks in homogeneous and isotropic materials is formulated in section 3, while the corresponding stress intensity factors are provided for validation purposes and further analyzed to investigate the interaction effects resulting from the idealized arrangements of infinitely periodic cracks. More advanced application examples are investigated to illustrate various size- and heterogeneity-effects on the elastic properties of mixed-mode cracks with arbitrarily branched geometries in anisotropic bimaterials.

2. Problem formulation

In the two-dimensional Cartesian coordinate system, the elastic field solutions due a network of periodically spaced dislocations with a inter-dislocation distance L are used to solve the boundary value problems of finite kinked and branched cracks in anisotropic bimaterials. For a single dislocation in bimaterials, which is not strictly located at the interfaces, the derivation

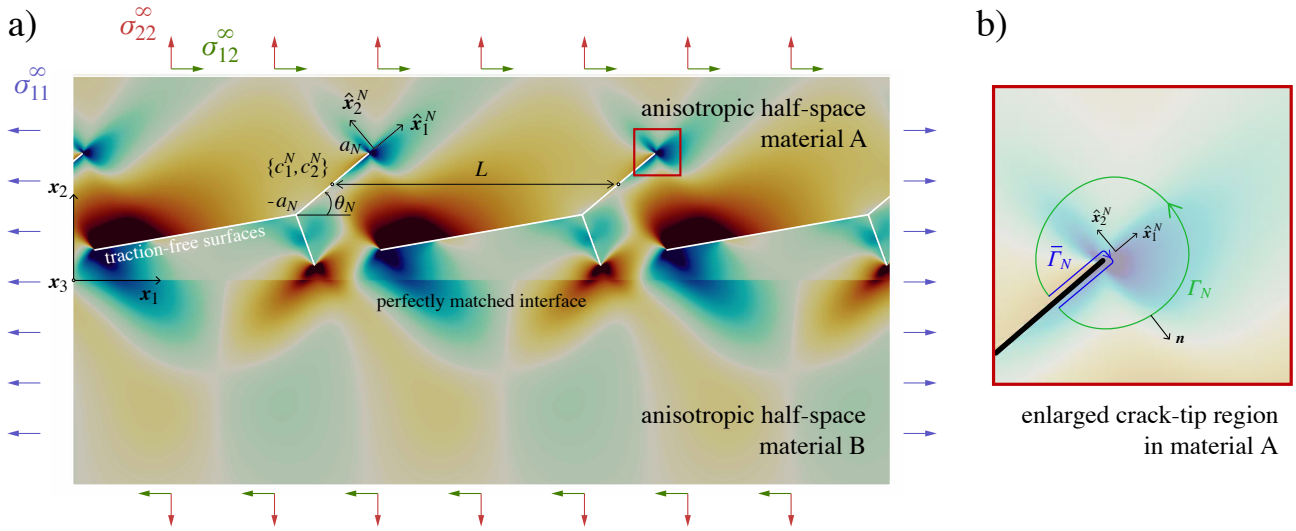

Figure 1: (a) An infinite periodically spaced network of branched cracks with three segments is embedded in the upper half space of an anisotropic bimaterial in presence of a perfectly bounded internal interface. The mismatch between both anisotropic elastic constants is taken into account, such that discontinuous stress components can be obtained by the present field solutions. (b) Definition of integration contours around a crack tip for evaluation of the path-independent J_k-integrals.

of the Green's functions has been presented by Barnett and Lothe (1974), Belov et al. (1983) and Ting (1992, 1996), while the dislocation arrays have been formulated by Chou et al. (1975), Hirth et al. (1979) and more recently by Chu and Pan (2014). Using the Green's functions for a dislocation array with arbitrary characters, the crack arrays are therefore considered as the continuous distributions of dislocations, for which the density of defects must fulfill the traction-free boundary conditions at the crack faces. The singular integral equations of Cauchy-type are obtained, and finally solved by the Gauss-Chebyshev quadrature scheme developed by Erdogan et al. (1973). From the field solutions, the contour J_k-integrals as crack propagation criterion are consistently evaluated along the crack tips of branched cracks. Although the present general formalism is dedicated to multiple straight crack segments with arbitrary geometries, such that the curved cracks can be suitably represented through a series of straight cracks, a particular attention is paid to kinked and forked cracks.

2.1. Stroh formalism and Green's functions for dislocation arrays in anisotropic bimaterials

As pictured in Fig. (1a), the bicrystals are formed by joining two linear anisotropic elastic materials A (upper material) and B (lower), which are defined by means of specific orientation relations along fixed crystal directions. The global and fixed coordinate system is conveniently defined by $(\mathrm{O}, \boldsymbol{x}_1, \boldsymbol{x}_2, \boldsymbol{x}_3)$, the perfectly matched interface is located at $x_2 = 0$, with $x_2 > 0$ for material A, and $x_2 < 0$ for material B. Without loss of generality, the individual dislocations are embedded in the upper material A, and are aligned with the $\boldsymbol{x}_3$-axis. The prescribed Burgers vector $\boldsymbol{b}_{\mathrm{A}}$ is the same in magnitude and direction for all dislocations, and is defined in two dimensions without screw dislocation components, such that $\boldsymbol{b}_{\mathrm{A}} = \left[b_{x_1}, b_{x_2}, 0\right]^{\mathrm{t}}$, in accordance with the present mixed-mode loading at long distances. The field stresses $\boldsymbol{\sigma}(x_1, x_2) = \sigma_{ij}(x_1, x_2)$ and the displacements $\boldsymbol{u}(x_1, x_2) = u_i(x_1, x_2)$ that are produced by the internal displacement jump in both half-spaces A and B are related by the full anisotropic Hooke law for constitutive relations, as follows

$$\sigma_{ij}\left(x_1, x_2\right) = c_{ijkl}(x_2)\, u_{k,l}\left(x_1, x_2\right), \tag{1}$$

where a comma stands for differentiation, with repeated indices denoting summation convention ranging from 1 to 3, unless stipulated otherwise. The anisotropic elastic constants of the fourth-order stiffness tensor are fully symmetric, i.e., $c_{ijkl} = c_{jikl} = c_{ijlk} = c_{klij}$, and the partial differential equation of mechanical equilibrium without body forces that is fulfilled in both crystals A and B in terms of the elastic displacement fields is given by

$$\begin{cases} {}_{\mathrm{A}}c_{ijkl}\ {}_{\mathrm{A}}u_{k,jl}\left(x_1, x_2\right) = 0 \\ {}_{\mathrm{B}}c_{ijkl}\ {}_{\mathrm{B}}u_{k,jl}\left(x_1, x_2\right) = 0, \end{cases} \tag{2}$$

where the elastic constants ${}_{\mathrm{A}}c_{ijkl}$ and ${}_{\mathrm{B}}c_{ijkl}$ are both defined by the local coordinates relative to the local crystal orientation and crystallography of each misoriented material. In the following, the pre-subscripts A and B in the elastic properties and also the field expressions will be omitted for clarity if no distinction between the dissimilar materials is required.

The displacement field in the upper material A produced by n extrinsic dislocations from $-\infty$ to ∞ is obtained by using the standard anisotropic elastic solution for a single dislocation and changing the dislocation location at (x_1^D, x_2^D) by $(x_1^D + nL, x_2^D)$, as already formulated (Chou et al., 1975, Chu and Pan, 2014, Hirth et al., 1979, Vattré and Pan, 2018). Thus, the summation of the displacement fields of the individual dislocations in A leads to the displacement fields due to an infinite dislocation network

parallel to the interface, ${}_{\rm A}u_k^{\text{array dis}}(x_1,x_2)$, with $k=\{1,2,3\}$, as follows

$$\begin{aligned}{}_{\rm A}\boldsymbol{u}^{\text{array dis}}(x_1,x_2;x_1^D,x_2^D) =& \frac{1}{\pi}\sum_{n=-\infty}^{\infty}\text{Im}\Big[{}_{\rm A}\mathbf{A}\left\langle\ln(x_1-(x_1^D+nL)+{}_{\rm A}p^{\dagger}(x_2-x_2^D))\right\rangle{}_{\rm A}\boldsymbol{q}^{\infty}\Big]\\ &+\frac{1}{\pi}\sum_{n=-\infty}^{\infty}\text{Im}\Big[\sum_{\alpha=1}^{3}{}_{\rm A}\mathbf{A}\left\langle\ln(x_1-(x_1^D+nL)+{}_{\rm A}p^{\dagger}x_2-{}_{\rm A}p_*^{\alpha}\,x_2^D)\right\rangle{}_{\rm A}\boldsymbol{q}^{\alpha}\Big],\end{aligned} \tag{3}$$

where ${}_*$ indicates complex conjugation. The complex matrices $\left\langle f(z^{\dagger})\right\rangle$ with a logarithmic form are introduced, i.e.

$$\left\langle f(z^{\dagger})\right\rangle=\text{diag}\big[f(z^1),f(z^2),f(z^3)\big]=\begin{bmatrix}f(z^1) & & \\ & f(z^2) & \\ & & f(z^3)\end{bmatrix}, \tag{4}$$

for which the symbol † is used to identify the element in the diagonal matrix. The first term in eq. (3) corresponds to the full-plane dislocation Green's functions in A, and both unknown constant vectors ${}_{\rm A}\boldsymbol{q}^{\infty}$ and ${}_{\rm A}\boldsymbol{q}^{\alpha}$ are determined by the perfectly matched interface conditions (Ting, 1996), as defined by

$$\begin{aligned}&{}_{\rm A}\boldsymbol{q}^{\infty}={}_{\rm A}\mathbf{H}^{\rm t}\,\boldsymbol{b}_{\rm A}\\ &{}_{\rm A}\boldsymbol{q}^{\alpha}=\underbrace{{}_{\rm A}\mathbf{A}^{-1}\left({}_{\rm A}\mathbf{M}+{}_{\rm B}\mathbf{M}_*\right)^{-1}\left({}_{\rm B}\mathbf{M}_*-{}_{\rm A}\mathbf{M}_*\right){}_{\rm A}\mathbf{A}_*}_{={}_{\rm AA}\mathbf{N}}\,\mathbf{I}^{\alpha}{}_{\rm A}\boldsymbol{q}_*^{\infty}={}_{\rm AA}\mathbf{N}\,\mathbf{I}^{\alpha}{}_{\rm A}\mathbf{H}_*^{\rm t}\,\boldsymbol{b}_{\rm A},\end{aligned} \tag{5}$$

where the diagonal matrices $\mathbf{I}^{\alpha}$ are defined by

$$\mathbf{I}^1=\text{diag}\big[1,0,0\big],\ \ \mathbf{I}^2=\text{diag}\big[0,1,0\big],\ \ \text{and,}\ \ \mathbf{I}^3=\text{diag}\big[0,0,1\big], \tag{6}$$

so that $\alpha=\{1,2,3\}$. In eqs. (3) and (5), the complex non-singular eigenmatrices ${}_{\rm A}\mathbf{A}=\big[{}_{\rm A}\boldsymbol{a}^1,{}_{\rm A}\boldsymbol{a}^2,{}_{\rm A}\boldsymbol{a}^3\big]$ are associated with the Stroh eigenvectors ${}_{\rm A}\boldsymbol{a}^{\alpha}$ as columns and the corresponding Stroh eigenvalues ${}_{\rm A}p^{\alpha}$ are obtained by solving the following eigensystem of equations, i.e.

$$\big[\mathbf{Q}+p\left(\mathbf{R}+\mathbf{R}^{\rm t}\right)+p^2\,\mathbf{T}\big]\,\boldsymbol{a}=\boldsymbol{\Pi}\,\boldsymbol{a}=\mathbf{0}, \tag{7}$$

by virtue of the standard eigenvalue problem in anisotropic elasticity theory (Stroh, 1958, 1962). In eq. (7), the superscript ${}^{\rm t}$ denotes the matrix transpose, while $\mathrm{Q}_{ik}=c_{i1k1}$, $\mathrm{R}_{ik}=c_{i1k2}$, and, $\mathrm{T}_{ik}=c_{i2k2}$, which are properly rotated with respect to the coordinate systems spanned by the $\boldsymbol{x}_1$- and $\boldsymbol{x}_2$- axes. A non-trivial solution can be found only if the determinant of $\boldsymbol{\Pi}$ is zero, i.e.

$$\det\boldsymbol{\Pi}=\mathbf{0}, \tag{8}$$

leading to a polynomial equation in p of degree six, with real coefficients. Due to the positive definiteness of elastic strain energy, the solutions of eq. (8) have six imaginary roots, which occur in complex conjugates (Eshelby et al., 1953). In particular, the roots are conveniently arranged such that the three first eigenvalue solutions p^{α} have positive imaginary parts, indexed by superscripts $\alpha=\{1,2,3\}$. The remaining three solutions have negative imaginary parts, so that $p^{\alpha+3}=p_*^{\alpha}$. The eigenvectors $\boldsymbol{a}^{\alpha}=a_k^{\alpha}$ are also complex conjugates with $\boldsymbol{a}^{\alpha+3}=\boldsymbol{a}_*^{\alpha}=a_{k_*}^{\alpha}$, so that ${}_{\rm A}\mathbf{A}_*$ in eq. (5) is defined by ${}_{\rm A}\mathbf{A}_*=\big[{}_{\rm A}\boldsymbol{a}_*^1,{}_{\rm A}\boldsymbol{a}_*^2,{}_{\rm A}\boldsymbol{a}_*^3\big]$.

Furthermore, the complex vectors $\boldsymbol{h}^{\alpha}$ of the subsidiary complex matrices ${}_{\rm A}\mathbf{H}=\big[{}_{\rm A}\boldsymbol{h}^1,{}_{\rm A}\boldsymbol{h}^2,{}_{\rm A}\boldsymbol{h}^3\big]$ in eq. (5) are related to the vectors $\boldsymbol{a}^{\alpha}$ by

$$p^{\alpha}\,\boldsymbol{h}^{\alpha}=p^{\alpha}\left(\mathbf{R}^{\rm t}+p^{\alpha}\,\mathbf{T}\right)\boldsymbol{a}^{\alpha}=-\left(\mathbf{Q}+p^{\alpha}\,\mathbf{R}\right)\boldsymbol{a}^{\alpha}, \tag{9}$$

while the eigenvectors $\boldsymbol{a}^{\alpha}$ and $\boldsymbol{h}^{\beta}$ satisfy the central normalization relations in the Stroh formalism, as follows

$$(\boldsymbol{h}^{\beta})^{\rm t}\,\boldsymbol{a}^{\alpha}+(\boldsymbol{a}^{\beta})^{\rm t}\,\boldsymbol{h}^{\alpha}=\delta_{\alpha\beta}, \tag{10}$$

with $\delta_{\alpha\beta}$ the 3×3 Kronecker delta. Futhermore, the displacement field in material B is given by

$${}_{\rm B}\boldsymbol{u}^{\text{array dis}}(x_1,x_2;x_1^D,x_2^D)=\frac{1}{\pi}\sum_{n=-\infty}^{\infty}\text{Im}\sum_{\alpha=1}^{3}{}_{\rm B}\mathbf{A}\left\langle\ln(x_1-(x_1^D+nL)+{}_{\rm B}p^{\dagger}x_2-{}_{\rm A}p^{\alpha}x_2^D)\right\rangle{}_{\rm B}\boldsymbol{q}^{\alpha}, \tag{11}$$

within which the eigenmatrix ${}_{\rm B}\mathbf{A}$ is accordingly associated with the Stroh eigenvalues ${}_{\rm B}p^{\alpha}$, while the unknown vectors ${}_{\rm B}\boldsymbol{q}^{\alpha}$ for perfect interfaces are given by

$${}_{\rm B}\boldsymbol{q}^{\alpha}=\underbrace{{}_{\rm B}\mathbf{A}^{-1}\left({}_{\rm A}\mathbf{M}_*+{}_{\rm B}\mathbf{M}\right)^{-1}\left({}_{\rm A}\mathbf{M}+{}_{\rm A}\mathbf{M}_*\right){}_{\rm A}\mathbf{A}}_{={}_{\rm BA}\mathbf{N}}\,\mathbf{I}^{\alpha}{}_{\rm A}\boldsymbol{q}^{\infty}={}_{\rm BA}\mathbf{N}\,\mathbf{I}^{\alpha}{}_{\rm A}\mathbf{H}^{\rm t}\,\boldsymbol{b}_{\rm A}, \tag{12}$$

where the positive-definite Hermitian impedance tensors ${}_{\chi}\mathbf{M}$ in eqs. (5) and (12) are defined by

$${}_{\chi}\mathbf{M}=-\,i\,{}_{\chi}\mathbf{H}\,{}_{\chi}\mathbf{A}^{-1}, \tag{13}$$

with $\chi = \{\mathrm{A}, \mathrm{B}\}$, while ${}_{\chi}\boldsymbol{h}^{\alpha} = i\,{}_{\chi}\mathbf{M}\,{}_{\chi}\boldsymbol{a}^{\alpha}$,which offers a second relation between the displacement with ${}_{\chi}\boldsymbol{a}^{\alpha}$ and the traction with ${}_{\chi}\boldsymbol{h}^{\alpha}$. Using index notation, the derivative of the displacement field components in A, given by eq. (3), with respect to the space coordinates is written as

$$\begin{aligned}{}_{\mathrm{A}}u^{\text{array dis}}_{k,l}(x_1,x_2;x_1^D,x_2^D) = \frac{1}{\pi}\sum_{n=-\infty}^{\infty}\mathrm{Im}\sum_{m=1}^{3}\Big[{}_{\mathrm{A}}\mathrm{A}_{km}\,{}_{\mathrm{A}}q_m^{\infty}\,(x_1-(x_1^D+nL)+{}_{\mathrm{A}}p^m(x_2-x_2^D))^{-1}\,(\delta_{l1}+{}_{\mathrm{A}}p^m\,\delta_{l2})\Big]\\ +\frac{1}{\pi}\sum_{n=-\infty}^{\infty}\mathrm{Im}\sum_{m=1}^{3}\Big[\sum_{\alpha=1}^{3}{}_{\mathrm{A}}\mathrm{A}_{km}\,{}_{\mathrm{A}}q_m^{\alpha}\,(x_1-(x_1^D+nL)+{}_{\mathrm{A}}p^m x_2-{}_{\mathrm{A}}p_*^{\alpha}\,x_2^D)^{-1}\,(\delta_{l1}+{}_{\mathrm{A}}p^m\,\delta_{l2})\Big],\end{aligned} \tag{14}$$

which can be summed to give strains. The sum in eq. (14) over n from $-\infty$ to ∞ has an explicit solution (Hirth et al., 1979, Morse and Feshbach, 1953), i.e.,

$$\sum_{n=-\infty}^{\infty}(z+nL)^{-1} = \frac{\pi}{L}\,\mathrm{ctg}\,\frac{\pi}{L}z, \tag{15}$$

so that eq. (14) can be expressed in a closed form as

$$\begin{aligned}{}_{\mathrm{A}}u^{\text{array dis}}_{k,l}(x_1,x_2;x_1^D,x_2^D) = \frac{1}{L}\mathrm{Im}\Big[{}_{\mathrm{A}}\mathrm{A}_{km}\,{}_{\mathrm{A}}q_m^{\infty}\,\mathrm{ctg}\Big(\frac{\pi}{L}\big(x_1-x_1^D+{}_{\mathrm{A}}p^m(x_2-x_2^D)\big)\Big)\,(\delta_{l1}+{}_{\mathrm{A}}p^m\,\delta_{l2})\Big]\\ +\frac{1}{L}\mathrm{Im}\sum_{\alpha=1}^{3}\Big[{}_{\mathrm{A}}\mathrm{A}_{km}\,{}_{\mathrm{A}}q_m^{\alpha}\,\mathrm{ctg}\Big(\frac{\pi}{L}\big(x_1-x_1^D+{}_{\mathrm{A}}p^m x_2-{}_{\mathrm{A}}p_*^{\alpha}\,x_2^D\big)\Big)\,(\delta_{l1}+{}_{\mathrm{A}}p^m\,\delta_{l2})\Big],\end{aligned} \tag{16}$$

where summation over the repeated index m is applied from 1 to 3, while the displacement gradients in B are analogously given by

$${}_{\mathrm{B}}u^{\text{array dis}}_{k,l}(x_1,x_2;x_1^D,x_2^D) = \frac{1}{L}\mathrm{Im}\sum_{\alpha=1}^{3}\Big[{}_{\mathrm{B}}\mathrm{A}_{km}\,{}_{\mathrm{B}}q_m^{\alpha}\,\mathrm{ctg}\Big(\frac{\pi}{L}\big(x_1-x_1^D+{}_{\mathrm{B}}p^m x_2-{}_{\mathrm{A}}p^{\alpha}x_2^D\big)\Big)\,(\delta_{l1}+{}_{\mathrm{B}}p^m\,\delta_{l2})\Big], \tag{17}$$

by differentiating eq. (11) with respect to the space coordinates. By virtue of the constitutive Hooke law in eq. (1), the stress state in material A can also determined, as follows

$$\begin{aligned}{}_{\mathrm{A}}\sigma^{\text{array dis}}_{ij}(x_1,x_2;x_1^D,x_2^D) = \frac{1}{L}\mathrm{Im}\Big[\big({}_{\mathrm{A}}c_{ijk1}+{}_{\mathrm{A}}p^m\,{}_{\mathrm{A}}c_{ijk2}\big)\,{}_{\mathrm{A}}\mathrm{A}_{km}\,{}_{\mathrm{A}}q_m^{\infty}\,\mathrm{ctg}\Big(\frac{\pi}{L}\big(x_1-x_1^D+{}_{\mathrm{A}}p^m(x_2-x_2^D)\big)\Big)\Big]\\ +\frac{1}{L}\mathrm{Im}\sum_{\alpha=1}^{3}\Big[\big({}_{\mathrm{A}}c_{ijk1}+{}_{\mathrm{A}}p^m\,{}_{\mathrm{A}}c_{ijk2}\big)\,{}_{\mathrm{A}}\mathrm{A}_{km}\,{}_{\mathrm{A}}q_m^{\alpha}\,\mathrm{ctg}\Big(\frac{\pi}{L}\big(x_1-x_1^D+{}_{\mathrm{A}}p^m x_2-{}_{\mathrm{A}}p_*^{\alpha}\,x_2^D\big)\Big)\Big],\end{aligned} \tag{18}$$

using eq. (1), while the stress fields in B are given by

$${}_{\mathrm{B}}\sigma^{\text{array dis}}_{ij}(x_1,x_2;x_1^D,x_2^D) = \frac{1}{L}\mathrm{Im}\sum_{\alpha=1}^{3}\Big[\big({}_{\mathrm{B}}c_{ijk1}+{}_{\mathrm{B}}p^m\,{}_{\mathrm{B}}c_{ijk2}\big)\,{}_{\mathrm{B}}\mathrm{A}_{km}\,{}_{\mathrm{B}}q_m^{\alpha}\,\mathrm{ctg}\Big(\frac{\pi}{L}\big(x_1-x_1^D+{}_{\mathrm{B}}p^m x_2-{}_{\mathrm{A}}p^{\alpha}x_2^D\big)\Big)\Big], \tag{19}$$

which result from the presence of an infinite periodically spaced arrays of lattice dislocations with inter-dislocation spacings L embedded in the upper material A.

2.2. The singular integral equations for a network of kinked and forked cracks

The two-dimensional boundary-value problem for kinked and forked cracks in anisotropic bimaterials is treated by use of continuous distribution of dislocations with specific Burgers vectors along each crack segment to be determined by the traction-free surface conditions (Bilby et al., 1955, Bilby and Eshelby, 1968, Bilby and Cardew, 1975, Hills et al., 1996). As illustrated in Fig. (1a), the elementary branched crack, which is composed of N_{Max} crack segments, with $N_{\text{Max}} = 2$, and $N_{\text{Max}} > 2$ for the kinked, and forked crack problem, respectively, and is also part of the infinite array of cracks is arbitrary oriented in the upper material A. Each rectilinear segment N, with $N = 1,\ldots,N_{\text{Max}}$, of the elementary branched crack is arbitrarily defined by θ_N the oriented angle between the horizontal $\boldsymbol{x}_1$-axis of the global coordinate system $(\boldsymbol{x}_1,\boldsymbol{x}_2)$ and the local $\hat{\boldsymbol{x}}_1^N$-axis, which is collinear with the crack segment. A local Cartesian coordinate system $(\hat{\boldsymbol{x}}_1^N,\hat{\boldsymbol{x}}_2^N)$ is also introduced and attached to each crack segment, centered at the point of coordinate $\{c_1^N,c_2^N\}$ with half crack-length a_N, subjected to an externally and uniformly applied stress field. These displacements are represented by unknown distributions of dislocation densities along each crack segment, which are determined by requiring that the traction-free surface conditions along the crack segments are fulfilled under plane strain conditions.

On the crack surfaces, the applied stress fields are therefore removed by the equivalent and opposite stresses produced by the sliding and opening displacement components from the crack arrays. The uniform load components σ_{ij}^{∞} applied at infinity are given by

$$\sigma_{ij}^{\infty} = \begin{bmatrix}\sigma_{11}^{\infty} & \sigma_{12}^{\infty} & 0\\ \sigma_{12}^{\infty} & \sigma_{22}^{\infty} & 0\\ 0 & 0 & 0\end{bmatrix}, \tag{20}$$

without loss of generality. The non-zero stress field components are conveniently expressed in the local axis of each crack segment N to

$$\begin{aligned}
\hat{\sigma}_{11}^{\infty N} &= \sigma_{11}^{\infty}\cos^2\theta_N + \sigma_{22}^{\infty}\sin^2\theta_N + 2\,\sigma_{12}^{\infty}\sin\theta_N\cos\theta_N\,,\\
\hat{\sigma}_{22}^{\infty N} &= \sigma_{11}^{\infty}\sin^2\theta_N + \sigma_{22}^{\infty}\cos^2\theta_N - 2\,\sigma_{12}^{\infty}\sin\theta_N\cos\theta_N\,,\\
\hat{\sigma}_{12}^{\infty N} &= (\sigma_{22}^{\infty} - \sigma_{11}^{\infty})\sin\theta_N\cos\theta_N + \sigma_{12}^{\infty}\cos 2\theta_N\,,
\end{aligned} \tag{21}$$

for which the superimposed symbol $\hat{}$ represents any quantities transformed into the local coordinate system of the N^{th} crack of interest. On the other hand, the corresponding stress field components produced by an array of extrinsic dislocations are given by introducing the vector ${}_{\text{A}}\boldsymbol{\tau}^{\text{array dis}}(x_1,x_2;x_1^D,x_2^D)$, as follows

$${}_{\text{A}}\boldsymbol{\tau}^{\text{array dis}}(x_1,x_2;x_1^D,x_2^D) = \Big[{}_{\text{A}}\sigma_{11}^{\text{array dis}}(x_1,x_2;x_1^D,x_2^D),\,{}_{\text{A}}\sigma_{22}^{\text{array dis}}(x_1,x_2;x_1^D,x_2^D),\,{}_{\text{A}}\sigma_{12}^{\text{array dis}}(x_1,x_2;x_1^D,x_2^D)\Big]^{\text{t}}, \tag{22}$$

which, according to eqs. (18) and (5), is written in matrix notation as

$$\begin{aligned}
{}_{\text{A}}\boldsymbol{\tau}^{\text{array dis}}(x_1,x_2;x_1^D,x_2^D) = {}& \frac{1}{L}\,\text{Im}\Big[{}_{\text{A}}\boldsymbol{\Lambda}^{\text{t}}\,{}_{\text{A}}\mathbf{A}\Big\langle \text{ctg}\Big(\frac{\pi}{L}\big(x_1 - x_1^D + {}_{\text{A}}p^{\dagger}(x_2 - x_2^D)\big)\Big)\Big\rangle\,{}_{\text{A}}\mathbf{H}^{\text{t}}\,\boldsymbol{b}_{\text{A}}\Big]\\
&+ \frac{1}{L}\,\text{Im}\sum_{\alpha=1}^{3}\Big[{}_{\text{A}}\boldsymbol{\Lambda}^{\text{t}}\,{}_{\text{A}}\mathbf{A}\Big\langle \text{ctg}\Big(\frac{\pi}{L}\big(x_1 - x_1^D + {}_{\text{A}}p^{\dagger}x_2 - {}_{\text{A}}p_*^{\alpha}\,x_2^D\big)\Big)\Big\rangle\,{}_{\text{AA}}\mathbf{N}\,\mathbf{I}^{\alpha}\,{}_{\text{A}}\mathbf{H}_*^{\text{t}}\,\boldsymbol{b}_{\text{A}}\Big],
\end{aligned} \tag{23}$$

where the elasticity-based matrix ${}_{\text{A}}\boldsymbol{\Lambda}_{3\times 3}$ is given by

$${}_{\text{A}}\boldsymbol{\Lambda} = \big[{}_{\text{A}}\text{Q}_{1k} + {}_{\text{A}}p^k\,{}_{\text{A}}\text{R}_{1k},\,{}_{\text{A}}\text{R}_{k2} + {}_{\text{A}}p^k\,{}_{\text{A}}\text{T}_{2k},\,{}_{\text{A}}\text{R}_{k1} + {}_{\text{A}}p^k\,{}_{\text{A}}\text{T}_{1k}\big]\,, \tag{24}$$

with $k = \{1,2,3\}$. Similarly to eq. (21), the shear and normal stress components produced by the dislocation networks are transformed from the global coordinate system to the local coordinate system dedicated to the specific N^{th} crack segment, by use of the Mohr transformation matrix $\mathbf{P}^N$, i.e.

$$\underbrace{\begin{bmatrix}{}_{\text{A}}\hat{\sigma}_{12}^{\text{array dis}\,N}(\hat{x}_1^N,\hat{x}_2^N;x_1^D,x_2^D)\\ {}_{\text{A}}\hat{\sigma}_{22}^{\text{array dis}\,N}(\hat{x}_1^N,\hat{x}_2^N;x_1^D,x_2^D)\end{bmatrix}}_{={}_{\text{A}}\hat{\boldsymbol{\tau}}^{\text{array dis}\,N}(\hat{x}_1^N,\hat{x}_2^N;x_1^D,x_2^D)} = \underbrace{\begin{bmatrix}-\sin\theta_N\cos\theta_N & \sin\theta_N\cos\theta_N & \cos 2\theta_N\\ \sin^2\theta_N & \cos^2\theta_N & -2\sin\theta_N\cos\theta_N\end{bmatrix}}_{=\mathbf{P}^N}\underbrace{\begin{bmatrix}{}_{\text{A}}\sigma_{11}^{\text{array dis}}(x_1,x_2;x_1^D,x_2^D)\\ {}_{\text{A}}\sigma_{22}^{\text{array dis}}(x_1,x_2;x_1^D,x_2^D)\\ {}_{\text{A}}\sigma_{12}^{\text{array dis}}(x_1,x_2;x_1^D,x_2^D)\end{bmatrix}}_{={}_{\text{A}}\boldsymbol{\tau}^{\text{array dis}}(x_1,x_2;x_1^D,x_2^D)}, \tag{25}$$

which are the only two components required to solve the branched crack problem. Here and in the following, the tilde symbol in subscripts represents the non-zero shear $_{12}$ and normal $_{22}$ components of the local traction stresses only, thus without the $_{11}$ component. Combining eq. (24) with eq. (25), the local traction stresses at $(\hat{x}_1^N,\hat{x}_2^N)$ become

$$\begin{aligned}
{}_{\text{A}}\hat{\boldsymbol{\tau}}^{\text{array dis}\,N}(\hat{x}_1^N,\hat{x}_2^N;x_1^D,x_2^D) = {}& \frac{1}{L}\,\text{Im}\Big[\mathbf{P}^N\,{}_{\text{A}}\boldsymbol{\Lambda}^{\text{t}}\,{}_{\text{A}}\mathbf{A}\Big\langle \text{ctg}\Big(\frac{\pi}{L}\big(x_1 - x_1^D + {}_{\text{A}}p^{\dagger}(x_2 - x_2^D)\big)\Big)\Big\rangle\,{}_{\text{A}}\mathbf{H}^{\text{t}}\,\boldsymbol{b}_{\text{A}}\Big]\\
&+ \frac{1}{L}\,\text{Im}\sum_{\alpha=1}^{3}\Big[\mathbf{P}^N\,{}_{\text{A}}\boldsymbol{\Lambda}^{\text{t}}\,{}_{\text{A}}\mathbf{A}\Big\langle \text{ctg}\Big(\frac{\pi}{L}\big(x_1 - x_1^D + {}_{\text{A}}p^{\dagger}x_2 - {}_{\text{A}}p_*^{\alpha}\,x_2^D\big)\Big)\Big\rangle\,{}_{\text{AA}}\mathbf{N}\,\mathbf{I}^{\alpha}\,{}_{\text{A}}\mathbf{H}_*^{\text{t}}\,\boldsymbol{b}_{\text{A}}\Big],
\end{aligned} \tag{26}$$

for which the discrete Burgers vectors $\boldsymbol{b}_{\text{A}}$ are located at $(x_1^D + nL, x_2^D)$ in the upper material A.

Following the concept of continuously distributed infinitesimal dislocations to analyze crack problems, the non-uniform displacements across surfaces are described in terms of continuous infinitesimal dislocations. The continuous distribution of dislocations is specified by a single-valued density function $\boldsymbol{B}(\hat{\eta})$ situated at point $\hat{\eta}$, such that $\boldsymbol{B}(\hat{\eta})d\hat{\eta}$ represents the total length of the Burgers vectors of the infinitesimal dislocations lying between the points $\hat{\eta}$ and $\hat{\eta}+d\hat{\eta}$ on the crack plane. These artificial and mathematical dislocations with infinitesimal Burgers vectors $d\boldsymbol{b}_{\text{A}} = \boldsymbol{B}_{\text{A}}(\hat{\eta})d\hat{\eta}$ are also conveniently used in eq. (23) to picture the present branched cracks. For any particular point located along the N^{th} crack segment among an arbitrary total number of segments N_{Max}, the shear and normal traction across the crack segment N in the local system is also obtained by superposing the self-interaction of all infinitesimal dislocations along the segment as well as the contribution from other segments $M \neq N$. In other words, these stress components at any point $(\hat{x}_1^N, \hat{x}_2^N = 0)$ on the N^{th} crack segment are therefore due to the integrated effect from all distributed dislocation densities and can be expressed in the form of Fredholm integral equations, as follows

$$\begin{aligned}
{}_{\text{A}}\hat{\boldsymbol{\tau}}^{\text{crack}\,N}(\hat{x}_1^N,\hat{x}_2^N = 0) = \frac{1}{L}\int_{-a_N}^{a_N}\Bigg\{ & \text{Im}\Big[\mathbf{P}^N\,{}_{\text{A}}\boldsymbol{\Lambda}^{\text{t}}\,{}_{\text{A}}\mathbf{A}\Big\langle \text{ctg}\Big(\frac{\pi}{L}\big(x_1^N - x_1^{D_N} + {}_{\text{A}}p^{\dagger}(x_2^N - x_2^{D_N})\big)\Big)\Big\rangle\,{}_{\text{A}}\mathbf{H}^{\text{t}}\,\boldsymbol{B}_{\text{A}}(\hat{\eta}_N)\Big]\\
&+ \text{Im}\sum_{\alpha=1}^{3}\Big[\mathbf{P}^N\,{}_{\text{A}}\boldsymbol{\Lambda}^{\text{t}}\,{}_{\text{A}}\mathbf{A}\Big\langle \text{ctg}\Big(\frac{\pi}{L}\big(x_1^N - x_1^{D_N} + {}_{\text{A}}p^{\dagger}x_2^N - {}_{\text{A}}p_*^{\alpha}\,x_2^{D_N}\big)\Big)\Big\rangle\,{}_{\text{AA}}\mathbf{N}\,\mathbf{I}^{\alpha}\,{}_{\text{A}}\mathbf{H}_*^{\text{t}}\,\boldsymbol{B}_{\text{A}}(\hat{\eta}_N)\Big]\Bigg\}\,d\hat{\eta}_N\\
&+ \frac{1}{L}\sum_{\substack{M=1\\M\neq N}}^{N_{\text{Max}}}\int_{-a_M}^{a_M}\Bigg\{ \frac{1}{L}\,\text{Im}\Big[\mathbf{P}^N\,{}_{\text{A}}\boldsymbol{\Lambda}^{\text{t}}\,{}_{\text{A}}\mathbf{A}\Big\langle \text{ctg}\Big(\frac{\pi}{L}\big(x_1^N - x_1^{D_M} + {}_{\text{A}}p^{\dagger}(x_2^N - x_2^{D_M})\big)\Big)\Big\rangle\,{}_{\text{A}}\mathbf{H}^{\text{t}}\,\boldsymbol{B}_{\text{A}}(\hat{\eta}_M)\Big]\\
&+ \text{Im}\sum_{\alpha=1}^{3}\Big[\mathbf{P}^N\,{}_{\text{A}}\boldsymbol{\Lambda}^{\text{t}}\,{}_{\text{A}}\mathbf{A}\Big\langle \text{ctg}\Big(\frac{\pi}{L}\big(x_1^N - x_1^{D_M} + {}_{\text{A}}p^{\dagger}x_2^N - {}_{\text{A}}p_*^{\alpha}\,x_2^{D_M}\big)\Big)\Big\rangle\,{}_{\text{AA}}\mathbf{N}\,\mathbf{I}^{\alpha}\,{}_{\text{A}}\mathbf{H}_*^{\text{t}}\,\boldsymbol{B}_{\text{A}}(\hat{\eta}_M)\Big]\Bigg\}\,d\hat{\eta}_M\,,
\end{aligned}$$

(27)

with respect to the local coordinates, where the parameters needed to compute the components of the diagonal matrices with cotangent terms are written with respect to coordinates of the crack segments, i.e.

$$\begin{cases} x_1^N = c_1^N + \hat{x}_1^N \cos\theta_N \\ x_2^N = c_2^N + \hat{x}_1^N \sin\theta_N \end{cases}, \text{ and, } \quad \begin{cases} x_1^{D_N} = c_1^N + \hat{\eta}_N \cos\theta_N \\ x_2^{D_N} = c_2^N + \hat{\eta}_N \sin\theta_N \\ x_1^{D_M} = c_1^M + \hat{\eta}_M \cos\theta_M \\ x_2^{D_M} = c_2^M + \hat{\eta}_M \sin\theta_M \,, \end{cases} \tag{28}$$

merely derived from geometrical characteristics. By virtue of the superposition principle, the applied remote stresses are combined with the traction solutions produced by the continuously distributed dislocation densities to determine the resultant stress state, and the essential corresponding traction-free condition along all crack segment N, with $N = 1, \ldots, N_{\text{Max}}$, reads

$$\forall\, |\hat{x}_1^N| < a_N : \begin{cases} 0 = \hat{\sigma}_{12}^{\infty\, N=1} + {}_{\text{A}}\hat{\sigma}_{12}^{\text{array}\, N=1}(\hat{x}_1^{N=1}, 0) \\ 0 = \hat{\sigma}_{22}^{\infty\, N=1} + {}_{\text{A}}\hat{\sigma}_{22}^{\text{array}\, N=1}(\hat{x}_1^{N=1}, 0) \\ \quad \vdots \\ 0 = \hat{\sigma}_{12}^{\infty\, N=N_{\text{Max}}} + {}_{\text{A}}\hat{\sigma}_{12}^{\text{array}\, N=N_{\text{Max}}}(\hat{x}_1^{N=N_{\text{Max}}}, 0) \\ 0 = \hat{\sigma}_{22}^{\infty\, N=N_{\text{Max}}} + {}_{\text{A}}\hat{\sigma}_{22}^{\text{array}\, N=N_{\text{Max}}}(\hat{x}_1^{N=N_{\text{Max}}}, 0) \,, \end{cases} \tag{29}$$

where the components $_{12}$ and $_{22}$ induced by the dislocation densities on the right-hand side are given by the integral relations in eq. (27). The absence of traction vector components along all cracks leads to $2N_{\text{Max}}$ equations, for $2N_{\text{Max}}$ unknowns, for which the system of integral equations that cannot be analytically solved by inversion. Before applying the numerical integration treatment in the next section 2.3 to solve complex crack configurations, the following scaling rules for the continuous variables are conveniently introduced as follows

$$\begin{cases} \hat{t} = \dfrac{\hat{x}_1^N}{a_N} \\ \hat{s} = \dfrac{\hat{\eta}_N}{a_N} = \dfrac{\hat{\eta}_M}{a_M} \,, \end{cases} \tag{30}$$

where $\hat{t} \in [-1, 1]$ and $\hat{s} \in [-1, 1]$ are dimensionless curvilinear coordinates along the crack segments. Furthermore, anticipating the inverse square root singularities at each end of each crack N, with $N = 1, \ldots, N_{\text{Max}}$, the unknowns Burgers vectors $\boldsymbol{B}_{\text{A}}(\hat{\eta}_N)$ in eq. (27) are also rewritten as $\boldsymbol{B}_{\text{A}}^N(\hat{s})$, and subsequently replaced by choosing the following interpolation functions, i.e.

$$\boldsymbol{B}_{\text{A}}(\hat{\eta}_N) = \boldsymbol{B}_{\text{A}}(\hat{\eta}_N(\hat{s})) = \boldsymbol{B}_{\text{A}}^N(\hat{s}) = \omega(\hat{s})\, \boldsymbol{\phi}^N(\hat{s}) = \left(1 - \hat{s}^2\right)^{-1/2} \boldsymbol{\phi}^N(\hat{s}) \,, \tag{31}$$

where $\omega(\hat{s})$ is the fundamental function that is continuously differentiable with one-sided derivative at the end points, while $\boldsymbol{\phi}^N(\hat{s})$ are nonsingular unknown functions that reflect the strength of singularities. In accordance with the Gauss-Chebyshev quadrature method, the interpolation functions are therefore related to the Chebyshev polynomials, such that eqs. (27−31) are also discretized by a series of algebraic relations to determine the suitable strength functions $\boldsymbol{\phi}^N(\hat{s})$ of the dislocation distributions for every crack segment N, as formulated in the following section.

2.3. Numerical solutions based on the Gauss-Chebyshev collocation method

The local displacements that are represented by the unknown distributions of dislocation densities $\boldsymbol{B}_{\text{A}}^N(\hat{s})$ along each crack segment, the unknown functions $\boldsymbol{\phi}^N(\hat{s})$ are determined by requiring that the traction-free state along the crack segments is fulfilled at a given and appropriate set of collocation points. These collocation points are are placed in between the integration points where the values of the sliding and opening displacement components are numerically computed. The total number of N_{Int} integration points imposed on the N^{th} crack branch and of $N_{\text{Int}} - 1$ collocation points are denoted by $\hat{s}_i$ and $\hat{t}_k$, with $i = 1, \ldots, N_{\text{Int}}$, and $k = 1, \ldots, N_{\text{Int}} - 1$, as defined by

$$\begin{cases} \hat{s}_i = \cos\left((i - 1/2)\,\pi / N_{\text{Int}}\right) \\ \hat{t}_k = \cos\left(k\,\pi / N_{\text{Int}}\right) \,, \end{cases} \tag{32}$$

respectively. The discrete collocation relations of the Fredholm-type integral equation with Cauchy kernel for the shear and normal traction across the crack segment N in eq. (27) are given in series form, $\forall\, k = 1, \ldots, N_{\text{Int}} - 1$, by

$$\begin{aligned} {}_{\text{A}}\hat{\boldsymbol{T}}^{\text{crack}\, N}(\hat{t}_k, 0) \simeq \frac{a_N}{L} \sum_{i=1}^{N_{\text{Int}}} W_i(\hat{s}_i) \Bigg\{ & \operatorname{Im}\Big[\mathbf{P}^N {}_{\text{A}}\boldsymbol{\Lambda}^{\text{t}} {}_{\text{A}}\mathbf{A} \Big\langle \operatorname{ctg}\Big(\frac{\pi}{L} \big(a_N(\hat{t}_k - \hat{s}_i)\cos\theta_N + {}_{\text{A}}p^{\dagger}\, a_N(\hat{t}_k - \hat{s}_i)\sin\theta_N \big) \Big) \Big\rangle {}_{\text{A}}\mathbf{H}^{\text{t}}\, \boldsymbol{\phi}^N(\hat{s}_i) \Big] \\ & + \operatorname{Im} \sum_{\alpha=1}^{3} \Big[\mathbf{P}^N {}_{\text{A}}\boldsymbol{\Lambda}^{\text{t}} {}_{\text{A}}\mathbf{A} \Big\langle \operatorname{ctg}\Big(\frac{\pi}{L} \big(a_N(\hat{t}_k - \hat{s}_i)\cos\theta_N + {}_{\text{A}}p^{\dagger}(c_2^N + a_N\hat{t}_k \sin\theta_N) - {}_{\text{A}}p_*^{\alpha}(c_2^N + a_N\hat{s}_i \sin\theta_N) \big) \Big) \Big\rangle {}_{\text{AA}}\mathbf{N}\, \mathbf{I}^{\alpha} {}_{\text{A}}\mathbf{H}_*^{\text{t}}\, \boldsymbol{\phi}^N(\hat{s}_i) \Big] \Bigg\} \\ & + \sum_{\substack{M=1 \\ M \neq N}}^{N_{\text{Max}}} \frac{a_M}{L} \sum_{i=1}^{N_{\text{Int}}} W_i(\hat{s}_i) \Bigg\{ \operatorname{Im}\Big[\mathbf{P}^N {}_{\text{A}}\boldsymbol{\Lambda}^{\text{t}} {}_{\text{A}}\mathbf{A} \Big\langle \operatorname{ctg}\Big(\frac{\pi}{L} \big((c_1^N - c_1^M + a_N\hat{t}_k\cos\theta_N - a_M\hat{s}_i\cos\theta_M) + {}_{\text{A}}p^{\dagger}(c_2^N - c_2^M + a_N\hat{t}_k \sin\theta_N - a_M\hat{s}_i \sin\theta_M) \big) \Big) \Big\rangle {}_{\text{A}}\mathbf{H}^{\text{t}}\, \boldsymbol{\phi}^M(\hat{s}_i) \Big] \\ & + \operatorname{Im} \sum_{\alpha=1}^{3} \Big[\mathbf{P}^N {}_{\text{A}}\boldsymbol{\Lambda}^{\text{t}} {}_{\text{A}}\mathbf{A} \Big\langle \operatorname{ctg}\Big(\frac{\pi}{L} \big((c_1^N - c_1^M + a_N\hat{t}_k\cos\theta_N - a_M\hat{s}_i\cos\theta_M) + {}_{\text{A}}p^{\dagger}(c_2^N + a_N\hat{t}_k \sin\theta_N) - {}_{\text{A}}p_*^{\alpha}(c_2^M + a_M\hat{s}_i \sin\theta_M) \big) \Big) \Big\rangle {}_{\text{AA}}\mathbf{N}\, \mathbf{I}^{\alpha} {}_{\text{A}}\mathbf{H}_*^{\text{t}}\, \boldsymbol{\phi}^M(\hat{s}_i) \Big] \Bigg\} , \end{aligned}$$

(33)

by use of eqs. (28) and (30−32), where $W_i(\hat{s}_i) = \pi/N_{\text{Int}}$ is the appropriate weight function with respect to the fundamental function $\omega(\hat{s}_i)$, as described by Erdogan et al. (1973). Furthermore, the corresponding net stress state on each segment N in eq. (33) is also reduced to a standard matrix equation, i.e.

$$\forall k = 1, \ldots, N_{\text{Int}} - 1 : \begin{cases} 0 = \hat{\sigma}_{12}^{\infty\, N=1} + {}_{\text{A}}\hat{\sigma}_{12}^{\text{crack}\, N=1}(\hat{t}_k, 0) \\ 0 = \hat{\sigma}_{22}^{\infty\, N=1} + {}_{\text{A}}\hat{\sigma}_{22}^{\text{crack}\, N=1}(\hat{t}_k, 0) \\ \quad \vdots \\ 0 = \hat{\sigma}_{12}^{\infty\, N=N_{\text{Max}}} + {}_{\text{A}}\hat{\sigma}_{12}^{\text{crack}\, N=N_{\text{Max}}}(\hat{t}_k, 0) \\ 0 = \hat{\sigma}_{22}^{\infty\, N=N_{\text{Max}}} + {}_{\text{A}}\hat{\sigma}_{22}^{\text{crack}\, N=N_{\text{Max}}}(\hat{t}_k, 0)\,, \end{cases} \tag{34}$$

where the relevant external and crack-induced stress contributions are given by eqs. (21) and (33), respectively. The latter includes the dislocation density strengths $\boldsymbol{\phi}^N(\hat{s}_i)$ that are also evaluated at the N_{Int} zeros of the Chebyshev polynomials of the first kind, while the crack tractions are specified at the N_{Int} zeros of the Chebyshev polynomials of the second kind. The traction-free boundary conditions provided by eq. (34) leads to an incomplete system of $2N_{\text{Max}}(N_{\text{Int}} - 1)$ equations, for $2N_{\text{Max}}N_{\text{Int}}$ unknowns, so that $2N_{\text{Max}}$ additional relations are needed to solve the system of equations. For a crack configuration with N segments, the specific unknowns are defined in the index notation by

$$\forall i = 1, \ldots, N_{\text{Int}} : \left\{ \phi_{\hat{x}_1}^1(\hat{s}_i), \phi_{\hat{x}_2}^1(\hat{s}_i), \ldots, \phi_{\hat{x}_1}^{N_{\text{Max}}}(\hat{s}_i), \phi_{\hat{x}_2}^{N_{\text{Max}}}(\hat{s}_i) \right\}, \tag{35}$$

such that $\boldsymbol{\phi}^N(\hat{s}_i) = \left[\phi_{\hat{x}_1}^N(\hat{s}_i), \phi_{\hat{x}_2}^N(\hat{s}_i), 0\right]^{\text{t}}$, where $\phi_{\hat{x}_1}^N(\hat{s}_i)$ and $\phi_{\hat{x}_2}^N(\hat{s}_i)$ are equivalent to the sliding and opening of the material across the local coordinate axis $\hat{x}_1$ and $\hat{x}_2$, respectively.

A consistent closure condition is used to prevent any perturbation of the external applied stress state at long range by the completely embedded cracks, formulated in the integral form as follows

$$\sum_{N=1}^{N_{\text{Max}}} \int_{-a_N}^{a_N} \boldsymbol{B}_{\text{A}}(\hat{\eta}_N)\, d\hat{\eta}_N = \boldsymbol{0}\,, \tag{36}$$

so that the total Burgers vector content along the branched cracks is zero, i.e. no net displacement occurs. In the discretized scheme, eq. (36) reads

$$\begin{cases} \sum_{N=1}^{N_{\text{Max}}} a_N \sum_{i=1}^{N_{\text{Int}}} W_i(\hat{s}_i)\, \phi_{\hat{x}_1}^N(\hat{s}_i) \;= 0 \\ \sum_{N=1}^{N_{\text{Max}}} a_N \sum_{i=1}^{N_{\text{Int}}} W_i(\hat{s}_i)\, \phi_{\hat{x}_2}^N(\hat{s}_i) \;= 0\,, \end{cases} \tag{37}$$

leading to two additional equations, after projection on the local coordinate axis $\hat{x}_1$ and $\hat{x}_2$, respectively. For problems dedicated to periodically spaced arrays of single cracks, thus without branched segments, the system that combines together eqs. (34) with (37) contains enough linearly dependent equations to solve the unknown dislocation density distributions defined by eq. (31) with eq. (35). For $N_{\text{Int}} \geq 2$, however, extra equations are needed, and two types of continuity constraints that have to be fulfilled at crack kinking and branching are defined, respectively, such that the collocation integral equations and the additional constraints close the system of equations.

For the specific configuration of kinked cracks, with $N_{\text{Int}} = 2$, the sliding and opening displacements are continuous at the kinking nodes between two adjacent crack segments, e.g., the principal segment indexed by $N = 1$ and the finite kinked segment by $N = 2$, for which the continuity condition is expressed as

$$\lim_{\hat{\eta}_1 \to a_1} \boldsymbol{B}_{\text{A}}(\hat{\eta}_1) = \lim_{\hat{\eta}_2 \to -a_2} \boldsymbol{B}_{\text{A}}(\hat{\eta}_2) \;\Rightarrow\; \lim_{\hat{s} \to 1} \boldsymbol{B}_{\text{A}}^1(\hat{s}) = \lim_{\hat{s} \to -1} \boldsymbol{B}_{\text{A}}^2(\hat{s})\,, \tag{38}$$

where the sign in $\hat{\eta}_N \to \pm a_N$ and $\hat{s} \to \pm 1$ depends on the left- and right- hand sides of the specific crack segment that is connected to the kink node. By virtue of the interpolation functions given by in eq. (31) in the normalized and discretized form, the equality of the dislocation densities at the kink locations from eq. (38) reads

$$\begin{cases} \lim_{\hat{s}_1 \to 1} \phi_{\hat{x}_1}^1(\hat{s}_1) = \lim_{\hat{s}_{N_{\text{Int}}} \to -1} \phi_{\hat{x}_1}^2(\hat{s}_{N_{\text{Int}}}) \\ \lim_{\hat{s}_1 \to 1} \phi_{\hat{x}_2}^1(\hat{s}_1) = \lim_{\hat{s}_{N_{\text{Int}}} \to -1} \phi_{\hat{x}_2}^2(\hat{s}_{N_{\text{Int}}})\,, \end{cases} \tag{39}$$

which yields two extra boundary conditions after projection. From the square-root asymptotic field analysis near the crack tips, the unknown functions $\{\phi_{\hat{x}_1}^N, \phi_{\hat{x}_2}^N\}$ remain finite at the end-points $\hat{s} \to \pm 1$, as follows

$$\begin{aligned} \lim_{\hat{s}_1 \to 1} \phi_{\hat{x}_j}^1(\hat{s}_1) &= \frac{1}{N_{\text{Int}}} \sum_{i=1}^{N_{\text{Int}}} \frac{\sin\left(\pi\left(2N_{\text{Int}} - 1\right)(2i-1)\,/\,(4N_{\text{Int}})\right)}{\sin\left(\pi\left(2i-1\right)/\left(4N_{\text{Int}}\right)\right)}\, \phi_{\hat{x}_j}^1(s_i)\,, \\ \lim_{\hat{s}_{N_{\text{Int}}} \to -1} \phi_{\hat{x}_j}^2(\hat{s}_{N_{\text{Int}}}) &= \frac{1}{N_{\text{Int}}} \sum_{i=1}^{N_{\text{Int}}} \frac{\sin\left(\pi\left(2N_{\text{Int}} - 1\right)(2i-1)\,/\,(4N_{\text{Int}})\right)}{\sin\left(\pi\left(2i-1\right)/\left(4N_{\text{Int}}\right)\right)}\, \phi_{\hat{x}_j}^2(s_{N_{\text{Int}}+1-i})\,, \end{aligned} \tag{40}$$

concisely obtained by the Krenk interpolation formulae (Hills et al., 1996, Krenk, 1975).

On the other hand, a stronger continuity constraint than the relations in eq. (39) is imposed at the branched nodes with multiple intersecting crack segments, when $N > 2$, by ensuring the amplitude of the singular dislocation density of the branch crack equal to zero at the point where all main and branched segments intersect, as suggested by Cleary and co-authors (Barr and Cleary, 1981, Narendran and Cleary, 1984) for application problems to rock fracture mechanics. Thus, eq. (39), for which the net opening and sliding displacements cancel out at crack barchning, becomes

$$\begin{cases} \lim\limits_{\hat{s}_1 \to 1} \phi^1_{\hat{x}_1}(\hat{s}_1) = \lim\limits_{\hat{s}_{N_{\text{Int}}} \to -1} \phi^2_{\hat{x}_1}(\hat{s}_{N_{\text{Int}}}) = \ldots = \lim\limits_{\hat{s}_{N_{\text{Int}}} \to -1} \phi^{N_{\text{Max}}-1}_{\hat{x}_1}(\hat{s}_{N_{\text{Int}}}) = 0 \\ \lim\limits_{\hat{s}_1 \to 1} \phi^1_{\hat{x}_2}(\hat{s}_1) = \lim\limits_{\hat{s}_{N_{\text{Int}}} \to -1} \phi^2_{\hat{x}_2}(\hat{s}_{N_{\text{Int}}}) = \ldots = \lim\limits_{\hat{s}_{N_{\text{Int}}} \to -1} \phi^{N_{\text{Max}}-1}_{\hat{x}_2}(\hat{s}_{N_{\text{Int}}}) = 0\,, \end{cases} \tag{41}$$

leading to $(2N_{\text{Max}} - 2)$ extra equations for the branched crack configurations. Combining the latter equations with the two relations in eq. (37) that guarantee the zero net Burgers vector condition as well as the $2N_{\text{Max}}(N_{\text{Int}} - 1)$ relations from eqs. (34), the complete system that is composed of $2N_{\text{Max}}$ linear equations can be solved and the corresponding unknowns in eq. (35) consistently be determined. Once the dislocation density distributions are known, the resultant stress fields $\sigma_{ij}^{\text{array crack}}(x_1, x_2)$ at any point in the upper material A is obtained as follows

$$\begin{aligned} {}_{\text{A}}\boldsymbol{\sigma}^{\text{array crack}}(x_1,x_2) \simeq \boldsymbol{\sigma}^{\infty} + \frac{\pi}{LN_{\text{Int}}} \sum_{N=1}^{N_{\text{Max}}} a_N \sum_{i=1}^{N_{\text{Int}}} \Bigg\{ & \text{Im}\Big[{}_{\text{A}}\boldsymbol{\Lambda}^{\text{t}}\, {}_{\text{A}}\mathbf{A} \Big\langle \text{ctg}\Big(\frac{\pi}{L}\big(x_1 - (c_1^N + a_N \hat{s}_i \cos\theta_N) + {}_{\text{A}}p^{\dagger}(x_2 - (c_2^N + a_N \hat{s}_i \sin\theta_N))\big)\Big) \Big\rangle\, {}_{\text{A}}\mathbf{H}^{\text{t}}\, \boldsymbol{\phi}^N(\hat{s}_i) \Big] \\ & + \text{Im} \sum_{\alpha=1}^{3} \Big[{}_{\text{A}}\boldsymbol{\Lambda}^{\text{t}}\, {}_{\text{A}}\mathbf{A} \Big\langle \text{ctg}\Big(\frac{\pi}{L}\big(x_1 - (c_1^N + a_N \hat{s}_i \cos\theta_N) + {}_{\text{A}}p^{\dagger} x_2 - {}_{\text{A}}p_*^{\alpha}(c_2^N + a_N \hat{s}_i \sin\theta_N)\big)\Big) \Big\rangle\, {}_{\text{AA}}\mathbf{N}\, \mathbf{I}^{\alpha}\, {}_{\text{A}}\mathbf{H}_*^{\text{t}}\, \boldsymbol{\phi}^N(\hat{s}_i) \Big] \Bigg\}, \end{aligned} \tag{42}$$

including the ${}_{\text{A}}\sigma_{33}^{\text{array crack}}(x_1, x_2)$ component, where ${}_{\text{AA}}\mathbf{N}$ and ${}_{\text{A}}\boldsymbol{\Lambda}$ are defined in eqs. (5) and (24), respectively. Furthermore, the corresponding stress state in material B is given by

$${}_{\text{B}}\boldsymbol{\sigma}^{\text{array crack}}(x_1,x_2) \simeq \boldsymbol{\sigma}^{\infty} + \frac{\pi}{LN_{\text{Int}}} \sum_{N=1}^{N_{\text{Max}}} a_N \sum_{i=1}^{N_{\text{Int}}} \Bigg\{ \text{Im} \sum_{\alpha=1}^{3} \Big[{}_{\text{B}}\boldsymbol{\Lambda}^{\text{t}}\, {}_{\text{B}}\mathbf{A} \Big\langle \text{ctg}\Big(\frac{\pi}{L}\big(x_1 - (c_1^N + a_N \hat{s}_i \cos\theta_N) + {}_{\text{B}}p^{\dagger} x_2 - {}_{\text{A}}p^{\alpha}(c_2^N + a_N \hat{s}_i \sin\theta_N)\big)\Big) \Big\rangle\, {}_{\text{BA}}\mathbf{N}\, \mathbf{I}^{\alpha}\, {}_{\text{A}}\mathbf{H}^{\text{t}}\, \boldsymbol{\phi}^N(\hat{s}_i) \Big] \Bigg\}, \tag{43}$$

where ${}_{\text{BA}}\mathbf{N}$ is defined in eq. (12), and the elasticity-based matrix ${}_{\text{B}}\boldsymbol{\Lambda}$ by

$${}_{\text{B}}\boldsymbol{\Lambda} = \big[{}_{\text{B}}\text{Q}_{1k} + {}_{\text{B}}p^k\, {}_{\text{B}}\text{R}_{1k},\, {}_{\text{B}}\text{R}_{k2} + {}_{\text{B}}p^k\, {}_{\text{B}}\text{T}_{2k},\, {}_{\text{B}}\text{R}_{k1} + {}_{\text{B}}p^k\, {}_{\text{B}}\text{T}_{1k} \big]\,, \tag{44}$$

while ${}_{\text{B}}\text{Q}_{ik} = {}_{\text{B}}c_{i1k1}$, ${}_{\text{B}}\text{R}_{ik} = {}_{\text{B}}c_{i1k2}$, and, ${}_{\text{B}}\text{T}_{ik} = {}_{\text{B}}c_{i2k2}$. In particular, eq. (42) is of vital importance for computing the J_k-integrals (Budiansky and Rice, 1973, Rice, 1968) and also predicting the crack growth of the different crack branches in anisotropic bimaterials.

2.4. Calculation of J_k-integrals for branched crack arrays in anisotropic bimaterials

Path-independent relations are widely used to determine the two-dimensional J_k-integral (Budiansky and Rice, 1973, Rice, 1968) as a criteria to predict crack growth direction (Hellen and Blackburn, 1975), where J_1 is the standard path-independent J-integral introduced by Rice (1968) that is related to the energy release rate per unit crack advance (Gurtin and Podio-Guidugli, 1996). On the other hand, J_2 is path-independent only by adding an extra nontrivial contribution on the crack faces (Herrmann and Herrmann, 1981), and is also required to the mechanical fields near the crack tips. Basically, for a two-dimensional elastic body containing a crack that lies in the direction of $\boldsymbol{x}_1$-axis, the expression of the J_k-integral components in the global coordinate system are

$$\begin{aligned} J_k^{\Gamma \to 0} &= \lim_{\Gamma \to 0} \oint_{\Gamma} \big(\underbrace{ {}_{\text{A}}W(x_1,x_2)\delta_{kj} - {}_{\text{A}}\sigma_{ij}^{\text{array crack}}(x_1,x_2)\, {}_{\text{A}}u_{i,k}^{\text{array crack}}(x_1,x_2) }_{= {}_{\text{A}}\mathbf{L}} \big) n_j \, d\Gamma \\ &= \lim_{\Gamma \to 0} \oint_{\Gamma} \big(\tfrac{1}{2}\, {}_{\text{A}}\sigma_{mn}^{\text{array crack}}(x_1,x_2)\, {}_{\text{A}}u_{m,n}^{\text{array crack}}(x_1,x_2)\, n_k - {}_{\text{A}}\sigma_{ij}^{\text{array crack}}(x_1,x_2)\, n_j\, {}_{\text{A}}u_{i,k}^{\text{array crack}}(x_1,x_2) \big) d\Gamma\,, \end{aligned} \tag{45}$$

where ${}_{\text{A}}\mathbf{L}$ is the Eshelby energy-momentum tensor (Eshelby, 1951), ${}_{\text{A}}W(x_1, x_2)$ is the strain energy density that is determined with respect of the Cartesian components of the stress and displacement gradient tensors from the previous section 2.3, and Γ is a contour in the (x_1, x_2) plane that encloses the crack tips, while n_j denotes the corresponding unit outward normal to Γ at (x_1, x_2). The equality in eq. (45) holds only when the contour Γ shrinks onto the crack tips $\Gamma \to 0$. However, if the contour Γ^N for the N^{th} crack segment does not tend to the tips, the integral relation in eq. (45) becomes

$$J_k^{\Gamma_N} = \int_{\Gamma_N} \big\{ \big(\tfrac{1}{2}\, {}_{\text{A}}\sigma_{mn}^{\text{array crack}}(x_1,x_2)\, {}_{\text{A}}u_{m,n}^{\text{array crack}}(x_1,x_2)\, \hat{n}_k - {}_{\text{A}}\sigma_{ij}^{\text{array crack}}(x_1,x_2)\, n_j \underbrace{\partial_{x_k\, {}_{\text{A}}} u_i^{\text{array crack}}(x_1,x_2)}_{= {}_{\text{A}}u_{i,k}^{\text{array crack}}(x_1,x_2)} \big\} d\Gamma - \int_{\Gamma_N} [\![{}_{\text{A}}W(x_1,x_2)]\!]_-^+ n_k \, d\Gamma \tag{46}$$

where $[\![{}_{\mathrm{A}}W(x_1,x_2)]\!]^{+}_{-}$ stands for the jump in the strain energy density across the crack faces $\bar{\Gamma}_N$, while the superscripts $\{-,+\}$ refer to the two half-space subdomains connected to the negative and positive crack faces with respect to the $\boldsymbol{x}_2$-axis. The additional integral energy-based term on the right-hand side must be taken into account on the crack faces, which vanishes for J_1, and also influences J_2 only. For kinked and forked cracks, eq. (46) is consistently transformed into the local coordinate system, as follows

$$\hat{J}_k^{\Gamma_N} = \int_{\Gamma_N} \left\{ \tfrac{1}{2}\, {}_{\mathrm{A}}\sigma_{mn}^{\text{array crack}}(x_1,x_2)\, {}_{\mathrm{A}}u_{m,n}^{\text{array crack}}(x_1,x_2)\, \hat{n}_k - {}_{\mathrm{A}}\sigma_{ij}^{\text{array crack}}(x_1,x_2)\, n_j\, \partial_{\hat{x}_k\,\mathrm{A}} u_i^{\text{array crack}}(x_1,x_2) \right\} d\Gamma - \underbrace{\int_{\bar{\Gamma}_N} [\![{}_{\mathrm{A}}W(x_1,x_2)]\!]^{+}_{-}\, \hat{n}_k\, d\Gamma}_{=-\hat{J}_{2\text{ex}}}, \tag{47}$$

where $\hat{n}_k = \cos\langle n_j, \hat{x}_k \rangle$ is the projection of n_j on the $\hat{x}_k$-axes. Furthermore, the gradient terms in eq. (47) are given by

$$\begin{bmatrix} \partial_{\hat{x}_1\,\mathrm{A}} u_i^{\text{array crack}}(x_1,x_2) \\ \partial_{\hat{x}_2\,\mathrm{A}} u_i^{\text{array crack}}(x_1,x_2) \end{bmatrix} = \begin{bmatrix} \cos\theta_N & \sin\theta_N \\ -\sin\theta_N & \cos\theta_N \end{bmatrix} \begin{bmatrix} \partial_{x_1\,\mathrm{A}} u_i^{\text{array crack}}(x_1,x_2) \\ \partial_{x_2\,\mathrm{A}} u_i^{\text{array crack}}(x_1,x_2) \end{bmatrix}, \tag{48}$$

with positive θ_N, so that both $J_1^{\Gamma_N}$- and $J_2^{\Gamma_N}$- integrals are defined by

$$\begin{cases} \hat{J}_1^{\Gamma_N} = \displaystyle\int_{\Gamma_N} \Big\{ \tfrac{1}{2} \cos\langle n_j, \hat{x}_1 \rangle\, {}_{\mathrm{A}}\sigma_{mn}^{\text{array crack}}(x_1,x_2)\, {}_{\mathrm{A}}u_{m,n}^{\text{array crack}}(x_1,x_2) \\ \qquad\qquad - {}_{\mathrm{A}}\sigma_{ij}^{\text{array crack}}(x_1,x_2)\, n_j \left(\cos\theta_N\, \partial_{x_1\,\mathrm{A}} u_i^{\text{array crack}}(x_1,x_2) + \sin\theta_N\, \partial_{x_2\,\mathrm{A}} u_i^{\text{array crack}}(x_1,x_2) \right) \Big\} d\Gamma \\ \hat{J}_2^{\Gamma_N} = \displaystyle\int_{\Gamma_N} \Big\{ \tfrac{1}{2} \cos\langle n_j, \hat{x}_2 \rangle\, {}_{\mathrm{A}}\sigma_{mn}^{\text{array crack}}(x_1,x_2)\, {}_{\mathrm{A}}u_{m,n}^{\text{array crack}}(x_1,x_2) \\ \qquad\qquad - {}_{\mathrm{A}}\sigma_{ij}^{\text{array crack}}(x_1,x_2)\, n_j \left(-\sin\theta_N\, \partial_{x_1\,\mathrm{A}} u_i^{\text{array crack}}(x_1,x_2) + \cos\theta_N\, \partial_{x_2\,\mathrm{A}} u_i^{\text{array crack}}(x_1,x_2) \right) \Big\} d\Gamma + \hat{J}_{2\text{ex}}, \end{cases} \tag{49}$$

where Γ_N is a circular path with suitable polar coordinates centered at crack tips of the N^{th} segment, while $\bar{\Gamma}_N$ in the integral term $\hat{J}_{2\text{ex}}$ from eq. (47) is a convenient rectangular contour along the crack lips of width r_0, as schematically shown in Fig. (1b). The latter is introduced in the calculation of $\hat{J}_2^{\Gamma_N}$ only, and corresponds to the vicinity of dislocation cores for which the present linear elasticity theory fails.

3. Numerical examples

Various application examples from the single kinked crack in isotropic homogeneous materials to the closely-spaced network of forked cracks in anisotropic bimaterials as well as some effects from the inter-crack spacings to the elastic heterogeneity are investigated. The former limiting case of single branched cracks is theoretically formulated and the corresponding asymptotic solutions are compared to existing results reported in the literature. The present solutions are numerically evaluated in terms of stress intensity factors $\hat{\boldsymbol{K}}$ and the path-independent $\hat{J}_k$-integrals using $N_{\text{Int}} = 256$ integration points, which give excellent results compared to the mathematical crack solutions from Kitagawa et al. (1975). The numerical accuracy of the the shear and normal tractions with the Gauss-Chebyshev quadrature scheme ranges from ten to twelve significant digits for both pure tensile and shear conditions at long range. Application examples are performed on Copper, which is moderately anisotropic, where the elastic constants are $c_{11} = 168.4$ GPa, $c_{12} = 121.4$ GPa, and $c_{44} = 75.4$ GPa, indexed in Voigt notation, while the dislocation core width is arbitrary given by the lattice parameter of Copper as $r_0 = 0.3615$ nm. Unless mentioned otherwise, the $\hat{\boldsymbol{K}}$- and $\hat{J}_k$-based quantities are normalized by $K_{\text{I}} = \sigma_0^{\infty}\sqrt{\pi a_1}$ and $J_{\text{I}} = K_{\text{I}}^2(1-\nu_{\text{iso}}^2)/E_{\text{iso}}$, where σ_0^{∞} is the constant tensile or shear stress applied at infinity, ν_{iso} is the Poisson ratio and E_{iso} is Young modulus, obtained using the Voigt averaging procedure.

3.1. The limiting problem of single kinked and forked cracks

Several theoretical studies have investigated the implications of crack kinking and forking to the fracture behavior of engineering materials, specially examined on the basis of elastic stress intensity factors. However, considerable discrepancies of the stress intensity factor solutions have been recognized in the literature, as stipulated by as mentioned by Bilby et al. (1977), Suresh and Shih (1986), and He and Hutchinson (1989), for instance. The results for a single crack in an isotropic and infinite medium from Bilby et al. (1977), using a plane theory of elasticity derived by Khrapkov (1971), are widely referenced by the fracture community.

Without completely repeating the entire derivation of the equations from the previous section 2, the unknown functions in eq. (35) are reduced to $4N_{\text{Int}}$ (to $6N_{\text{Int}}$) for the kinked $*$ (forked $**$) crack problems, which can also be determined by solving $4N_{\text{Int}}-4$ ($6N_{\text{Int}}-6$) linear equations from eq. (34), respectively, as follows

$$\forall\, k = 1,\ldots,N_{\text{Int}}-1: \;\; ** \left\{ * \begin{cases} 0 = \hat{\sigma}_{12}^{\infty\,N=1} + {}_{\mathrm{A}}\hat{\sigma}_{12}^{\text{crack}\,N=1}(\hat{t}_k,0) \\ 0 = \hat{\sigma}_{22}^{\infty\,N=1} + {}_{\mathrm{A}}\hat{\sigma}_{22}^{\text{crack}\,N=1}(\hat{t}_k,0) \\ 0 = \hat{\sigma}_{12}^{\infty\,N=2} + {}_{\mathrm{A}}\hat{\sigma}_{12}^{\text{crack}\,N=2}(\hat{t}_k,0) \\ 0 = \hat{\sigma}_{22}^{\infty\,N=2} + {}_{\mathrm{A}}\hat{\sigma}_{22}^{\text{crack}\,N=2}(\hat{t}_k,0) \end{cases} \right. \\ \left. \begin{cases} 0 = \hat{\sigma}_{12}^{\infty\,N=3} + {}_{\mathrm{A}}\hat{\sigma}_{12}^{\text{crack}\,N=3}(\hat{t}_k,0) \\ 0 = \hat{\sigma}_{22}^{\infty\,N=3} + {}_{\mathrm{A}}\hat{\sigma}_{22}^{\text{crack}\,N=3}(\hat{t}_k,0), \end{cases} \right. \tag{50}$$

combined with 2 additional equations given by eq. (37), plus 2 (4) more relations by eqs. (39) and (41) with the aid of eq. (40) to complete the system $*$ $(**)$. The limiting problem of single kinked and forked cracks is also analyzed by use of the standard limit when $L \to \infty$, i.e.

$$\lim_{L\to\infty} \frac{1}{L} \operatorname{ctg} \frac{\pi}{L} z = (\pi z)^{-1}, \tag{51}$$

such that the crack-induced stress fields in eq. (50) are obtained by reducing eq. (33) to

$$\begin{aligned}
{}_{\mathrm{A}}\hat{\boldsymbol{\tau}}^{\text{single crack } N}(\hat{t}_k,0) \simeq \frac{a_N}{N_{\text{Int}}} \sum_{i=1}^{N_{\text{Int}}} \Bigg\{ & \operatorname{Im}\Big[\mathbf{P}^N {}_{\mathrm{A}}\boldsymbol{\Lambda}^{\mathrm{t}} {}_{\mathrm{A}}\mathbf{A} \Big\langle \big(a_N(\hat{t}_k - \hat{s}_i)\cos\theta_N + {}_{\mathrm{A}}p^{\dagger} a_N(\hat{t}_k - \hat{s}_i)\sin\theta_N \big)^{-1} \Big\rangle {}_{\mathrm{A}}\mathbf{H}^{\mathrm{t}} \boldsymbol{\phi}^N(\hat{s}_i) \Big] \\
& + \operatorname{Im} \sum_{\alpha=1}^{3} \Big[\mathbf{P}^N {}_{\mathrm{A}}\boldsymbol{\Lambda}^{\mathrm{t}} {}_{\mathrm{A}}\mathbf{A} \Big\langle \big(a_N(\hat{t}_k - \hat{s}_i)\cos\theta_N + {}_{\mathrm{A}}p^{\dagger}(c_2^N + a_N \hat{t}_k \sin\theta_N) - {}_{\mathrm{A}}p_*^{\alpha}(c_2^N + a_N \hat{s}_i \sin\theta_N) \big)^{-1} \Big\rangle {}_{\mathrm{AA}}\mathbf{N}\,\mathbf{I}^{\alpha} {}_{\mathrm{A}}\mathbf{H}_*^{\mathrm{t}} \boldsymbol{\phi}^N(\hat{s}_i) \Big] \Bigg\} \\
& + \frac{1}{N_{\text{Int}}} \sum_{\substack{M=1 \\ M\neq N}}^{N_{\text{Max}}} a_M \sum_{i=1}^{N_{\text{Int}}} \Bigg\{ \operatorname{Im}\Big[\mathbf{P}^N {}_{\mathrm{A}}\boldsymbol{\Lambda}^{\mathrm{t}} {}_{\mathrm{A}}\mathbf{A} \Big\langle \big((c_1^N - c_1^M + a_N \hat{t}_k \cos\theta_N - a_M \hat{s}_i \cos\theta_M) + {}_{\mathrm{A}}p^{\dagger}(c_2^N - c_2^M + a_N \hat{t}_k \sin\theta_N - a_M \hat{s}_i \sin\theta_M) \big)^{-1} \Big\rangle {}_{\mathrm{A}}\mathbf{H}^{\mathrm{t}} \boldsymbol{\phi}^M(\hat{s}_i) \Big] \\
& + \operatorname{Im} \sum_{\alpha=1}^{3} \Big[\mathbf{P}^N {}_{\mathrm{A}}\boldsymbol{\Lambda}^{\mathrm{t}} {}_{\mathrm{A}}\mathbf{A} \Big\langle \big((c_1^N - c_1^M + a_N \hat{t}_k \cos\theta_N - a_M \hat{s}_i \cos\theta_M) + {}_{\mathrm{A}}p^{\dagger}(c_2^N + a_N \hat{t}_k \sin\theta_N) - {}_{\mathrm{A}}p_*^{\alpha}(c_2^M + a_M \hat{s}_i \sin\theta_M) \big)^{-1} \Big\rangle {}_{\mathrm{AA}}\mathbf{N}\,\mathbf{I}^{\alpha} {}_{\mathrm{A}}\mathbf{H}_*^{\mathrm{t}} \boldsymbol{\phi}^M(\hat{s}_i) \Big] \Bigg\},
\end{aligned} \tag{52}$$

with $N_{\text{Max}} = 2$ $(*)$ or $= 3$ $(**)$, respectively, for which the associated stress components ${}_{12}$ and ${}_{22}$ are arranged as the term on the left-hand side of eq. (25). Once the system is solved and the corresponding vectorial unknowns $\{\boldsymbol{\phi}^N(\hat{s}_i)\}$, with $i = 1, \ldots, N_{\text{Int}}$, are determined, eq. (42) is used to calculate the mixed-mode stress intensity factors ${}_{\mathrm{A}}\hat{\boldsymbol{K}}^N$ in the suitable local coordinate system affiliated to the tips of the N^{th} crack, as follows

$$\begin{aligned}
{}_{\mathrm{A}}\hat{\boldsymbol{K}}^N = \begin{bmatrix} {}_{\mathrm{A}}\hat{K}_2^N \\ {}_{\mathrm{A}}\hat{K}_1^N \\ {}_{\mathrm{A}}\hat{K}_3^N \end{bmatrix} &= \lim_{\hat{x}_1 \to \pm a_N} \sqrt{2\pi(\pm a_N - \hat{x}_1)} \underbrace{\begin{bmatrix} \cos\theta_N & \sin\theta_N & 0 \\ -\sin\theta_N & \cos\theta_N & 0 \\ 0 & 0 & 1 \end{bmatrix}}_{=\boldsymbol{\Omega}_{3\times 3}^N} \underbrace{\begin{bmatrix} {}_{\mathrm{A}}\sigma_{12}^{\text{single crack } N}(\hat{x}_1^N, 0) \\ {}_{\mathrm{A}}\sigma_{22}^{\text{single crack } N}(\hat{x}_1^N, 0) \\ {}_{\mathrm{A}}\sigma_{32}^{\text{single crack } N}(\hat{x}_1^N, 0) = 0 \end{bmatrix}}_{={}_{\mathrm{A}}\boldsymbol{\tau}^{\text{single array } N}(\hat{t},0)} \\
&= \pm\sqrt{2\pi a_N}\, \boldsymbol{\Omega}_{3\times 3}^N \Big\{ \lim_{\hat{t}\to\pm 1} \sqrt{1 \mp \hat{t}}\ {}_{\mathrm{A}}\boldsymbol{\tau}^{\text{single array } N}(\hat{t}, 0) \Big\},
\end{aligned} \tag{53}$$

thus ${}_{\mathrm{A}}\hat{K}_3^N = 0$, in the present work. By applying eq. (51) to eq. (18), the shear and normal stress components produced by a single dislocation are also given by

$$\begin{aligned}
{}_{\mathrm{A}}\sigma_{i2}^{\text{array dis}}(x_1, x_2; x_1^D, x_2^D) = & \frac{1}{\pi} \operatorname{Im}\Big[\big(x_1 - x_1^D + {}_{\mathrm{A}}p^m (x_2 - x_2^D) \big)^{-1} \big({}_{\mathrm{A}}\mathrm{R}_{ki} + {}_{\mathrm{A}}p^m {}_{\mathrm{A}}\mathrm{T}_{ik} \big) {}_{\mathrm{A}}\mathrm{A}_{km}\, {}_{\mathrm{A}}q_m^{\infty} \Big] \\
& + \frac{1}{\pi} \operatorname{Im} \sum_{\alpha=1}^{3} \Big[\big(x_1 - x_1^D + {}_{\mathrm{A}}p^m x_2 - {}_{\mathrm{A}}p_*^{\alpha}\, x_2^D \big)^{-1} \big({}_{\mathrm{A}}\mathrm{Q}_{ik} + {}_{\mathrm{A}}p^m {}_{\mathrm{A}}\mathrm{T}_{ik} \big) {}_{\mathrm{A}}\mathrm{A}_{km}\, {}_{\mathrm{A}}q_m^{\alpha} \Big],
\end{aligned} \tag{54}$$

so that the curly bracketed part in eq. (53) is obtained by considering the integrated effect from all distributed dislocation densities, and also including eqs. (5), (9) and (31) into eq. (54). For the crack tip on the right-hand side of the N^{th} segment, i.e. for positive $\hat{t}$, the bracketed term in eq. (53) reads

$$\begin{aligned}
\lim_{\hat{t}\to 1} \sqrt{1-\hat{t}}\ {}_{\mathrm{A}}\boldsymbol{\tau}^{\text{single crack } N}(\hat{t}) = & \frac{1}{\pi} \operatorname{Im}\Bigg[{}_{\mathrm{A}}\mathbf{H}\, {}_{\mathrm{A}}\mathbf{H}^{\mathrm{t}} \Big\{ \lim_{\hat{t}\to 1} \sqrt{1-\hat{t}}\ \int_{-1}^{1} \frac{\boldsymbol{B}_{\mathrm{A}}^N(\hat{s})}{\hat{t}-\hat{s}} d\hat{s} \Big\} \Bigg] \\
& + \frac{1}{\pi} \operatorname{Im} \sum_{\alpha=1}^{3} \Bigg[{}_{\mathrm{A}}\mathbf{H}\, {}_{\mathrm{AA}}\mathbf{N}\,\mathbf{I}^{\alpha} {}_{\mathrm{A}}\mathbf{H}_*^{\mathrm{t}} \Big\{ \lim_{\hat{t}\to 1} \sqrt{1-\hat{t}}\ \int_{-1}^{1} \frac{\boldsymbol{B}_{\mathrm{A}}^N(\hat{s})}{\hat{t}-\hat{s}} d\hat{s} \Big\} \Bigg] \Bigg],
\end{aligned} \tag{55}$$

within which the limits of the integral fonctions with Cauchy kernels can be explicitly evaluated (Hills et al., 1996, Huang and Kardomateas, 2001, Yang and Yang, 2000), as follows

$$\lim_{\hat{t}\to 1} \sqrt{1-\hat{t}}\ \int_{-1}^{1} \frac{\boldsymbol{B}_{\mathrm{A}}^N(\hat{s})}{\hat{t}-\hat{s}} d\hat{s} = \frac{\pi}{\sqrt{2}}\, \boldsymbol{\phi}^N(+1), \tag{56}$$

with $\boldsymbol{\phi}^N(+1) = \big[\phi_{\hat{x}_1}^N(+1),\, \phi_{\hat{x}_2}^N(+1),\, 0\big]^{\mathrm{t}}$. Similar expression for the left-hand side of the tips are similarly derived for negative $\hat{t}$, so that eq. (53) reads

$$\begin{aligned}
{}_{\mathrm{A}}\hat{\boldsymbol{K}}^N = \begin{bmatrix} {}_{\mathrm{A}}\hat{K}_2^N \\ {}_{\mathrm{A}}\hat{K}_1^N \\ {}_{\mathrm{A}}\hat{K}_3^N = 0 \end{bmatrix} = \pm\sqrt{\pi a_N}\, \boldsymbol{\Omega}_{3\times 3}^N \Big\{ \operatorname{Im}\Big[{}_{\mathrm{A}}\mathbf{H}\, {}_{\mathrm{A}}\mathbf{H}^{\mathrm{t}}\, \boldsymbol{\phi}^N(\pm 1) + \sum_{\alpha=1}^{3} \big[{}_{\mathrm{A}}\mathbf{H}\, {}_{\mathrm{AA}}\mathbf{N}\,\mathbf{I}^{\alpha} {}_{\mathrm{A}}\mathbf{H}_*^{\mathrm{t}}\, \boldsymbol{\phi}^N(\pm 1) \big] \Big] \Big\},
\end{aligned} \tag{57}$$

where the finite values at the end-points, i.e.

$$\boldsymbol{\phi}^N(\pm 1) = \big[\phi_{\hat{x}_1}^N(\pm 1),\, \phi_{\hat{x}_2}^N(\pm 1),\, 0\big]^{\mathrm{t}}, \tag{58}$$

are obtained by the Krenk interpolation formulas in eq. (40).

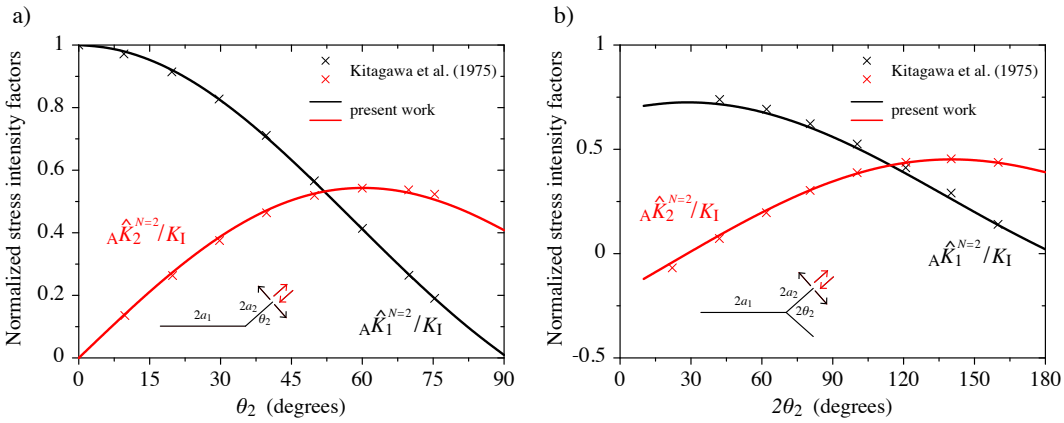

Figure 2: Variation of normalized ${}_{\rm A}\hat{K}_1^{N=2}$ and ${}_{\rm A}\hat{K}_2^{N=2}$ with the induced (a) kinked and (b) forked angle θ_2 under uniform tension, and comparison with the results from Kitagawa et al. (1975) for $a_2/a_1 = 0.1$, while $K_{\rm I}$ is the nominal stress intensity factor.

3.2. Validation with existing results reported in the literature

The limiting case for single kinked and branched cracks in two-dimensional elastically homogeneous and isotropic materials is investigated for validation purposes, for which the isotropic elastic constants are obtained using the Voigt averaging procedure. Under uniaxial uniform traction, the mixed-mode stress intensity factors are normalized by the corresponding nominal stress intensity factor $K_{\rm I} = \sigma_{22}^{\infty}\sqrt{\pi\ell}$ for a straight crack, where the crack length ℓ is projected in the direction perpendicular to the tensile $\boldsymbol{x}_2$-axis, so that $\ell = a_1 + a_2\cos\theta_2$, with $\theta_1 = 0^\circ$ and $a_2/a_1 = 0.1$. The variations of the normalized stress intensity factors ${}_{\rm A}\hat{K}_1^{N=2}$ and ${}_{\rm A}\hat{K}_2^{N=2}$ with respect to the kinked and forked angle θ_2 are shown in Fig. (2a) and (b), respectively. The present solutions are in excellent agreement with the results introduced by Kitagawa et al. (1975), also presented by Suresh and Shih (1986). In particular, the maximum value of ${}_{\rm A}\hat{K}_1^{N=2}$ for the kinked cracks is found using isotropic elasticity at $\theta_2 = 60.1^\circ$, while the in-plane shear mode vanishes at $2\theta_2 = 28.4^\circ$, as similarly obtained by Bilby et al. (1977).

3.3. Effect of the anisotropic elasticity under pure tensile and shear conditions

The previous configuration of kinked cracks, with $\theta_1 = 0^\circ$ and $a_2/a_1 = 0.1$, is used to analyze the effect of anisotropic elasticity in the field solutions, as focused in Fig. (3). Here and in the following, the superscripts N and subscripts A in the $\hat{\boldsymbol{K}}$- and $\hat{J}_k$-based quantities will be omitted for clarity in the figure legends since the schematics explicitly illustrate where these tip quantities are evaluated. The solid (dotted) lines represent the $\hat{\boldsymbol{K}}$- and $\hat{J}_k$-based results obtained by the anisotropic (isotropic) elasticity theory under pure traction and shear loadings at long range.

The differences between isotropic and anisotropic elasticity under traction occur for large values of θ_2, i.e., $\theta_2 > 40^\circ$ and $\theta_2 > 25^\circ$ for $\hat{K}_1$ and $\hat{K}_2$, respectively, as illustrated in Fig. (3a). The maximum value of $\hat{K}_2$ using anisotropic elasticity corresponds to $\theta_2 = 69.1^\circ$, which also differs from the isotropic calculation with $\theta_2 = 60.1^\circ$. On the other hand, Fig. (3b) shows that the stress intensity factor $\hat{K}_2$ for pure shear possesses two maximum values in magnitude with opposite sign, which reveal the crack-opening stress state under tension for negative values of θ_2. The anisotropic elasticity tends to decrease the magnitudes of $\hat{K}_1$ and $\hat{K}_2$ for the kinked cracks under shear loads, especially for the large kinked angles, when $|\theta_2| > 30^\circ$.

The $\hat{J}_k$-integrals in Fig. (3c) and (d) exhibit more significant quantitative and qualitative differences between isotropic and anisotropic results than the stress intensity factors $\hat{\boldsymbol{K}}$. For instance, the maximum magnitude in the J_1-integrals for pure shear occurs at $\hat{J}_{1\,\max} = \pm 59.4^\circ$ ($= \pm 58.9^\circ$) using anisotropic (isotropic) elasticity, which differs from the commonly used zero-$\hat{K}_2$ criterion for finite kinked cracks since $\hat{K}_2 = 0$ occurs at $\theta_2 = \pm 66.9^\circ$ ($\pm 70.3^\circ$). Interestingly, $\hat{J}_1'(\theta_2 = 0^\circ) = 0$ and $\hat{J}_1''(\theta_2 = 0^\circ) < 0$, for the anisotropic case, where $'$ denotes the derivative with respect to θ_2, while $\hat{J}_1'(\theta_2 = 0^\circ) = 0$ and $\hat{J}_1''(\theta_2 = 0^\circ) > 0$, for the isotropic case under shear loads.

Overall, the extra $\hat{J}_{2\,\rm ex}$ terms in the $\hat{J}_k$-integrals, as developped in section 2.4, are non-zero for all presented crack configurations. The $\hat{J}_2$-integrals also play a critical role in the $\hat{J}$-integral evaluations (Lee, 1986), as defined by $\hat{J} = (\hat{J}_1^2 + \hat{J}_2^2)^{-1/2}$, while the corresponding maximum magnitude of $\hat{J}_{\max}$ is found to occur when $\theta_2 = 21.6^\circ$ ($= 16.9^\circ$) using the anisotropic (isotropic) elasticity calculation under traction, as pictured by $*$ in Fig. (3c), while $\hat{J}_{1\,\max}$ occurs at $\theta_2 = 0^\circ$. The criterion based on the $\hat{J}$-integrals also means that the actual path is not a pure mode-I path, which may also have significant consequences in predicting of the crack stability as well as the directions of crack propagation as the compared with the well-know $\hat{J}_1$-integrals in relation with the corresponding maximum energy-release rates for cracks in anisotropic solids. Under shear loads, $\hat{J}_{\max} = \pm 42.6^\circ$ and $\pm 37.4^\circ$ using anisotropic and isotropic solutions, respectively, exhibiting further discrepancies performed by use of the isotropic approximation in the elastic material properties.

According to the aforementioned fracture criteria, the most significant dissimilarity among the predictions occurs when the loading is related to pure shears, for which the zero-$\hat{K}_2$ criterion as a fracture criterion for finite kinked cracks in anisotropic solids is very questionable.

3.4. Effect of the crack length ratios

Figure (4) illustrates the influence of the a_2/a_1 ratio on the stress intensity factors $\hat{\boldsymbol{K}}$ as well as the $\hat{J}_k$-integral calculations. The previous results with $a_2/a_1 = 0.1$ are pictured with dotted lines for comparison, while the field solutions for $a_2/a_1 = 1$ are

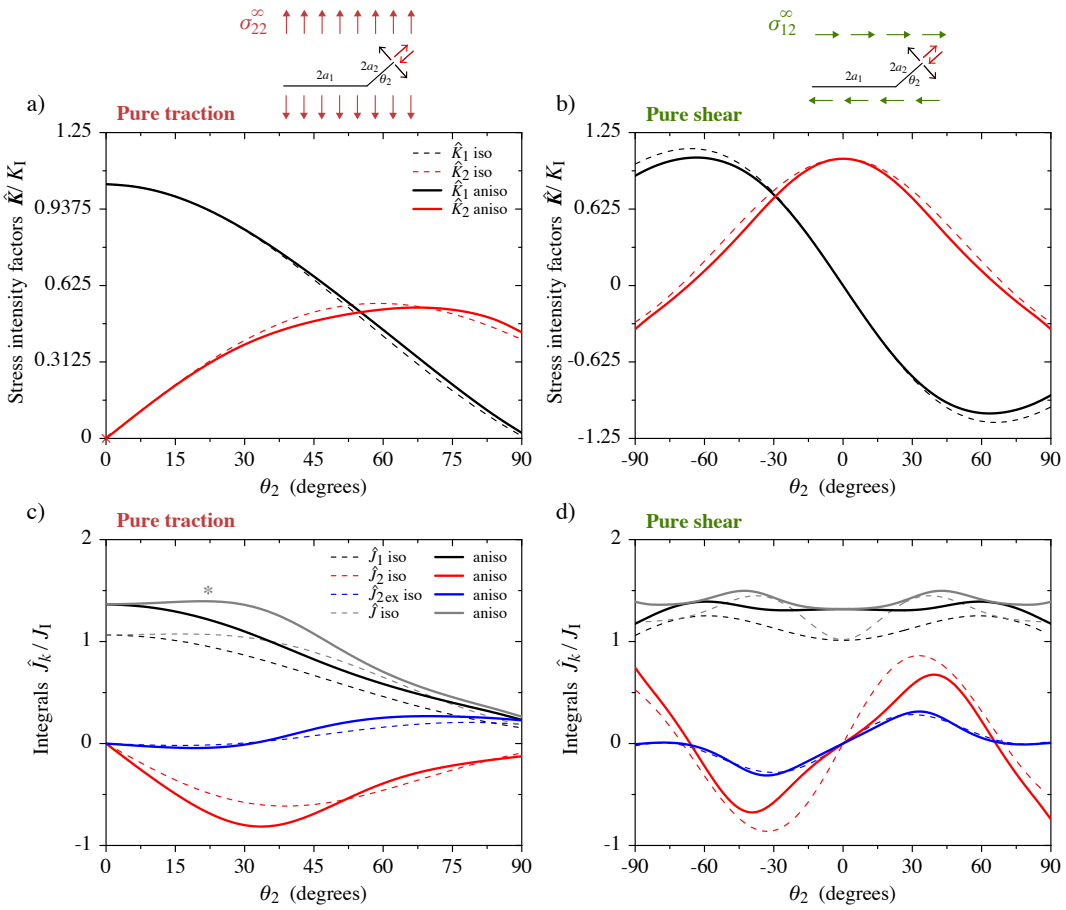

Figure 3: Effect of the anisotropic elasticity on the stress intensity factors $\hat{\boldsymbol{K}}$ and $\hat{J}_k$-integrals for kinked cracks under pure tensile and shear conditions.

depicted with solid lines. When $\theta_2 < 79.5^\circ$, $\hat{K}_1$ becomes negative for the pure traction case with $a_2/a_1 = 1$, as pictured by $*$ in Fig. (4a), meaning that the kinked crack tip closes and values of $\hat{K}_1$ for greater values of $\theta_2 > 79.5^\circ$ are invalid. The shear loading case in Fig. (4b) shows that the zero-$\hat{K}_2$ criterion is satisfied for $\theta_2 = \pm 50.4^\circ$, which can also be compared to $\pm 66.9^\circ$ for $a_2/a_1 = 0.1$. Such significant difference demonstrates the great importance in considering the finite size of kinked cracks in appropriate crack problems as well as the possible hazards that can emerge when comparing the present results with solutions from asymptotic and perturbation analysis.

According to Fig. (4c) and (d), the maximum $\hat{J}_1$-integral magnitudes are reached when $\theta_2 = 0^\circ$ for both external loads using anisotropic elasticity theory, which also dramatically differ from the previous prediction based on the zero-$\hat{K}_2$ evaluation for the pure shear case. Clearly, such further discrepancy indicates that the $\hat{\boldsymbol{K}}$-based criteria are debatable as the fracture criteria for finite-length branched cracks. On the other hand, the previous comment on the discrepancies resulting from the $\hat{J}$- versus $\hat{J}_1$-integral criteria is even more evident for the case with equal lengths in both traction or shear loads, mainly due to the effect of $\hat{J}_2$-terms that exhibit more oscillating characteristics for $a_2/a_1 = 1$ with respect to θ_2 than the solutions with $a_2/a_1 = 0.1$.

3.5. Effect of the inter-crack spacings

The second size effect in Fig. (5a) and (b) is related to the influence on the $\hat{J}_k$-integrals of the inter-crack spacings L of the kinked crack arrays with $a_2/a_1 = 0.1$, under pure tensile and shear conditions, respectively. The dotted lines represent the calculations for single kinked cracks in anisotropic materials, thus for $L \to \infty$, while the corresponding arrays of closely-spaced cracks with $L = 5a_1/2$ and $\theta_1 = 0^\circ$ are depicted by solid lines. For information, the particular crack configuration with $L = 2a_1$ and $\theta_2 \neq 0^\circ$, corresponds to a crack network that cuts horizontally the entire solids. The amplitude of both $\hat{J}_1$- and $\hat{J}_2$-integrals increases with decreasing L for both loading conditions. While the trends of the variations are qualitatively unchanged for the pure traction case in Fig. (5a), the influence of L is more noticeable for the shear loads. For instance, $\hat{J}_{1\max}$ and $\hat{J}_{\max}$ occur at $\theta_2 \pm 48.0^\circ$ and $\pm 36.9^\circ$ for the network of cracks, compared to $\pm 59.4^\circ$ and $\pm 42.6^\circ$ for the single kinked cracks in anisotropic material, respectively. Without of need for extensive statistical aspects, this significant difference shows that the present ideal elastic interactions between the cracks at short range are also relevant to take into account for applications to crack coalescence and more generally, to the problem of effective elastic properties of anisotropic solids containing specific crack arrangements and densities with mixed-mode interactions. Furthermore, $\hat{J}_1'(\theta_2 = 0^\circ) = 0$ and $\hat{J}_1''(\theta_2 = 0^\circ) > 0$ for the network of cracks under shear loads, which exhibits a change of sign of $\hat{J}_1''$ compared with the corresponding single crack case.

3.6. Effect of heterogeneity on the elastic properties

Figure (6) illustrates the influence of elastic interaction that arises from the mismatch of the elastic properties on the $\hat{J}_k$-integrals for both the single kinked crack configuration as well as the infinite arrays of kinked cracks under pure shear loads. As

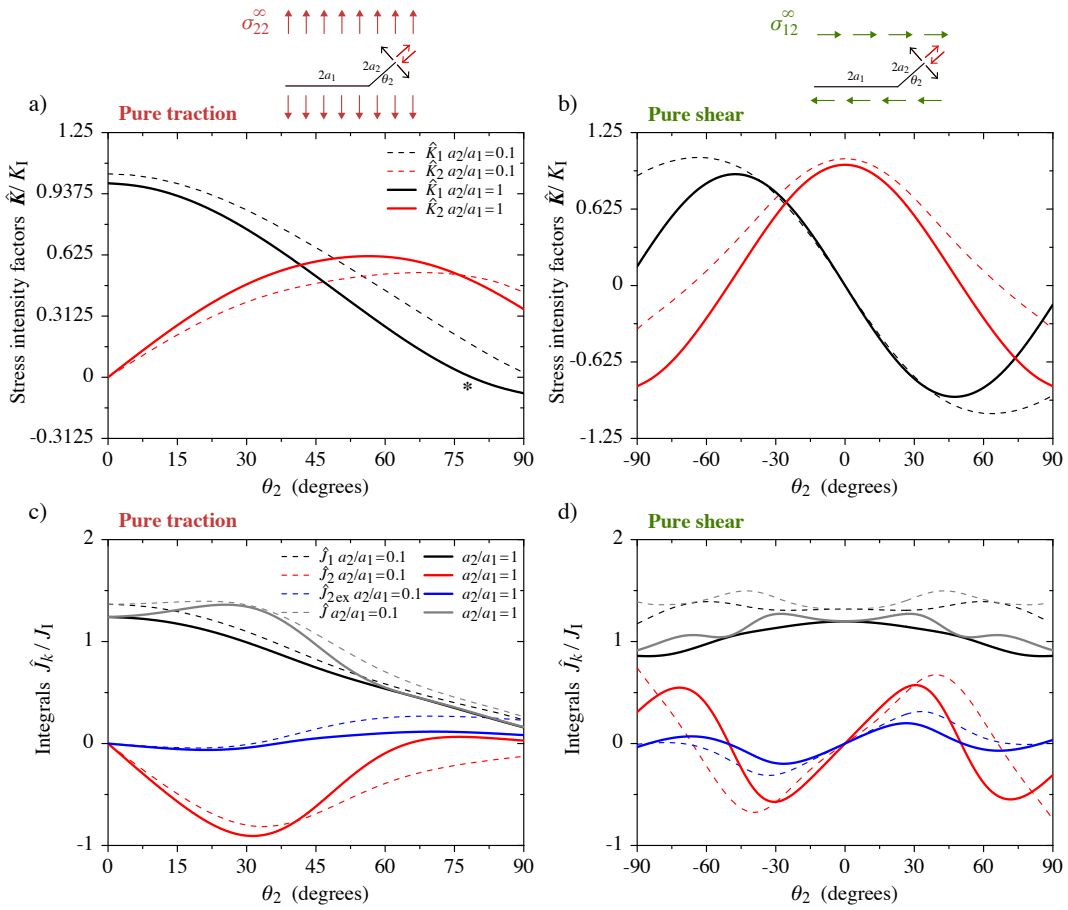

Figure 4: Effect of of the crack length ratio on the stress intensity factors $\hat{\boldsymbol{K}}$ and $\hat{J}_k$-integrals for kinked cracks under pure tensile and shear conditions.

illustrated in Fig. (1a), the elastic mismatch leads to a discontinuity in the in-plane stresses, for which the magnitude increases by increasing material mismatch of the anisotropic bimaterials. The results are presented for $\theta_1 = 0^\circ$ and $a_2/a_1 = 0.1$, as previously, while $c_2^{N=2} = a_1/5$, for which the tip of the kinked segment is therefore close to the interface when $\theta_2 = -90^\circ$. The elastic properties in the upper material A are fixed, while the elastic constants of the lower material B are fictitiously multiplied or divided by three. In comparison with the previous solutions using homogeneous elasticity, as pictured by dotted lines, the $\hat{J}_k$ profiles are asymmetrical with respect to $\theta_2 = 0^\circ$, as shown by solid lines, especially for the $\hat{J}_1$-integrals. In accordance with Fig. (4b), for which the valid tensile opening mode with $\hat{K}_1 > 0$ is related to $\theta_2 < 0^\circ$, thus with a kinked segment taken downward towards material B, the driving force by evaluating $\hat{J}_1$ at the kinked tips for the single crack is larger for the case where material B is softer, thus in turn, when material A is stiffer, by comparing Fig. (6a) and (b). The kinked crack part is also attracted to the soft materials. For elastically soft material B, the $\hat{J}_1$ and $\hat{J}$ components reach maximum values in Fig. (6b) when the kinked segment is located at $\theta_2 = -73.3^\circ$ and -56.8°, respectively, while $\hat{J}_{1\,\max}$ and $\hat{J}_{\max}$ occur at $\theta_2 = -58.6^\circ$ and -46.1° for an infinity network with closely spaced cracks, as shown in Fig. (6c).

3.7. The linear elastic problem of single and closely-spaced forked cracks

As illustrated by the schematics in Fig. (7), the single forked crack in the homogeneous anisotropic material is composed of three finite-length segments, for which two segments are fixed, i.e., crack 1 and crack 3, arbitrarily oriented with $\theta_1 = 0^\circ$ and $\theta_3 = 60^\circ$, while θ_2 varies from -120° to 20°. Furthermore, a_1 and a_2 are fixed as well, with $a_2/a_1 = 0.1$, and different configurations with three lengths for a_3 are investigated, i.e., $a_3 = a_2/2$ (case 1), $a_3 = a_2$ (case 2), and $a_3 = 2a_2$ (case 3).

Figure (7a) shows that $\hat{K}_1$ cancels at $\theta_2 = -92.4^\circ$ for crack 2 and becomes negative below for the three cases. When $\theta_2 > -60^\circ$, $\hat{K}_1$ becomes increasingly sensitive as crack 2 approaches crack 3, while the magnitude is larger as the length a_3 is smaller. Furthermore, $\hat{K}_2$ varies quadratically with θ_2 for crack 2, until a change of sign for larger angles. From all results in terms of the stress intensity factors on crack 3, $\hat{K}_1$ becomes negative for case 3 of the smallest a_3 when $\theta_2 > -8.4^\circ$, while the other $\hat{\boldsymbol{K}}$-based quantities vary more monotonically, as illustrated Fig. (7b). Figure (7c) shows that the closer crack 2 is to crack 3, the larger the magnitude of $\hat{J}_1$, while $\hat{J}_2$ reaches a maximum magnitude at $\theta_2 = -30.9^\circ$, -35.5°, and -39.6°, for case 1, 2, and 3, respectively, before becoming negative for $\theta_2 = 1.7^\circ$, -1.5°, -9.3°, respectively. Interestingly, both $\hat{J}_1$- and $\hat{J}_2$-integrals for crack 3 behave oppositely in sign until the magnitudes converge to almost zero for the largest of θ_2, for instance when $\theta_2 > -14.1^\circ$ for case 1, as depicted by Fig. (7d).

The most advanced application example of the present formalism is introduced in Fig. (8), illustrating the effects of both inter-crack spacings and elastic mismatch on the $\hat{J}_k$-integrals at two extreme tips of forked crack 2 and crack 3 in homogeneous and heterogeneous materials under traction. The specific case 2 from Fig. (7) is treated, thus with $a_2/a_1 = a_2/a_3$ and $\theta_2 = 60^\circ$, while θ_2 varies from -120° to 20°. For comparison, the dotted lines are associated with simplified crack configurations. According

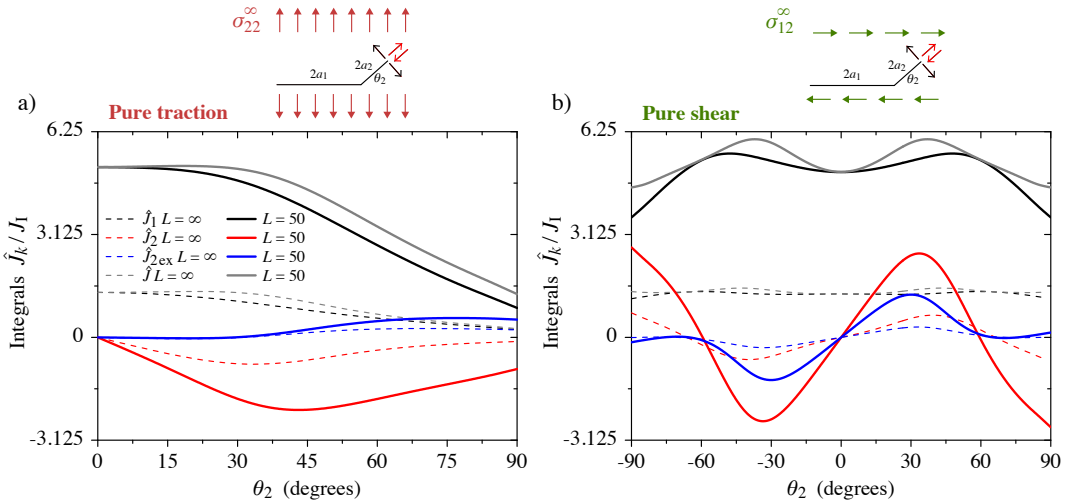

Figure 5: Effect of the inter-crack spacings on the $\hat{J}_k$-integral evaluation for kinked cracks under pure tensile and shear conditions. The single kinked crack is depicted with dotted lines, while the closely-spaced network of kinked cracks is illustrated using solid lines.

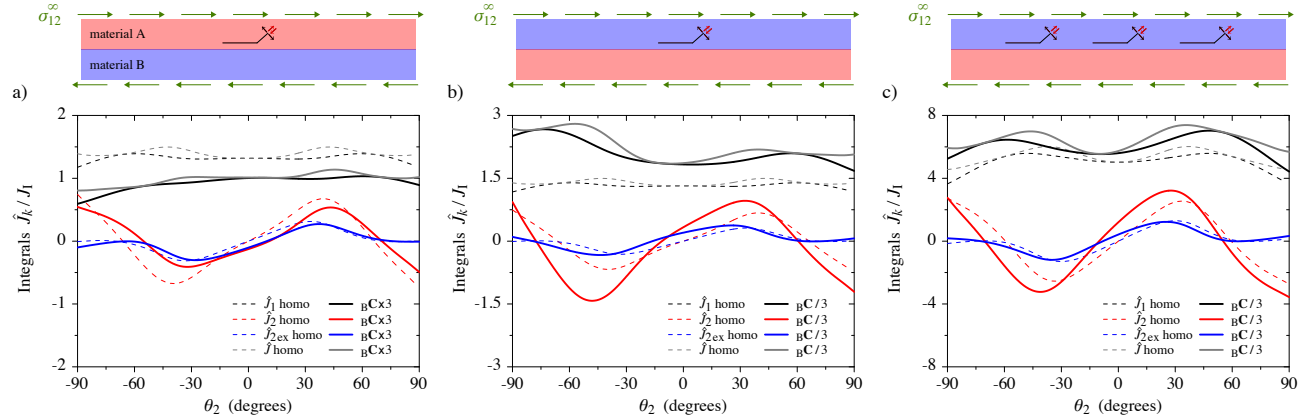

Figure 6: Effect of the heterogeneous elasticity on the $\hat{J}_k$-integral evaluation for a single kinked crack as well an infinite network of kinked cracks under pure shear loads. The elastic mismatch is introduced by fictitiously multiplied or divided by three the elastic constants of the lower material B.

to Fig. (8a), the closer crack 2 is to crack 3, the higher the $\hat{J}_1$ amplitude of the former crack 2, so that crack 3 enhances the propagation of crack 2 for the largest values of θ_2. This situation is more pronounced in the case of crack network. In particular, the $\hat{J}_k$-based quantities for crack 2 are small in magnitude when crack 2 is diametrically opposed to the former crack 3. On the contrary, Fig. (8b) shows that the $\hat{J}_k$-based quantities for crack 3 tend towards zero when the crack 2 is closest to the fixed crack 3, which corresponds to a stress state of crack 3 that is partly shielded by the elastic stress field produced by the crack 2. Figures (8c) and (d) demonstrate that the elastic heterogeneity only plays a role on crack 2, while the elastic mismatch has also no effect on the behavior of the crack 3. Interestingly, the elastic mismatch leads to the presence of a zero derivative for $\hat{J}_1$, resulting in the maximum value of $\hat{J}_{1\,\max}$ at $\theta_2 = -18.9^\circ$ for crack 2, as pictured by $*$ in Fig. (8c). This specific state does not exist in the homogeneous elasticity context, and the corresponding non-zero and dimensionless stress components, defined by $\sigma_{ij}^{\text{array crack}}(x_1, x_2)/\sigma_{22}^{\infty}$, are plotted in Fig. (9a), for illustration. Figure (9b) shows the corresponding variation of stresses along the vertical dotted lines displayed in Fig. (9a). In particular, Fig. (9a) and (b) depict the large discontinuities of the in-plane stress component $_{11}$ across both crack and interface planes as well as the traction-free conditions for $_{22}$ and $_{12}$ along the main crack plane that are therefore fully satisfied, as required.

4. Concluding remarks

Using the Stroh formalism to the anisotropic elasticity theory of extrinsic dislocations, the two-dimensional fracture problem of multiple branched crack arrays in anisotropic bimaterials is formulated by means of coupled integral equations. These equations are related to the arbitrarily-oriented configurations of infinitely periodic cracks in dissimilar orthotropic half-spaces under arbitrary far-field stress loading conditions, combined with appropriate boundary conditions in terms of dislocation density distributions along the crack segments. The full-field solutions for kinked and forked crack arrays are solved by employing the Gauss-Chebyshev quadrature and collocation formulae on Chebyshev nodes, while the limiting case of individual cracks in homogeneous and isotropic materials is theoretically derived for validation and comparison purposes. Explicit expressions of the local stress intensity factors for the single branched cracks in anisotropic bimaterials are obtained by interpolation, for which the results of the asymptotic limiting case are in excellent agreement with existing solutions reported in the literature. The path-independent J_k-integrals as crack propagation criterion are subsequently evaluated for mixed-mode crack configurations

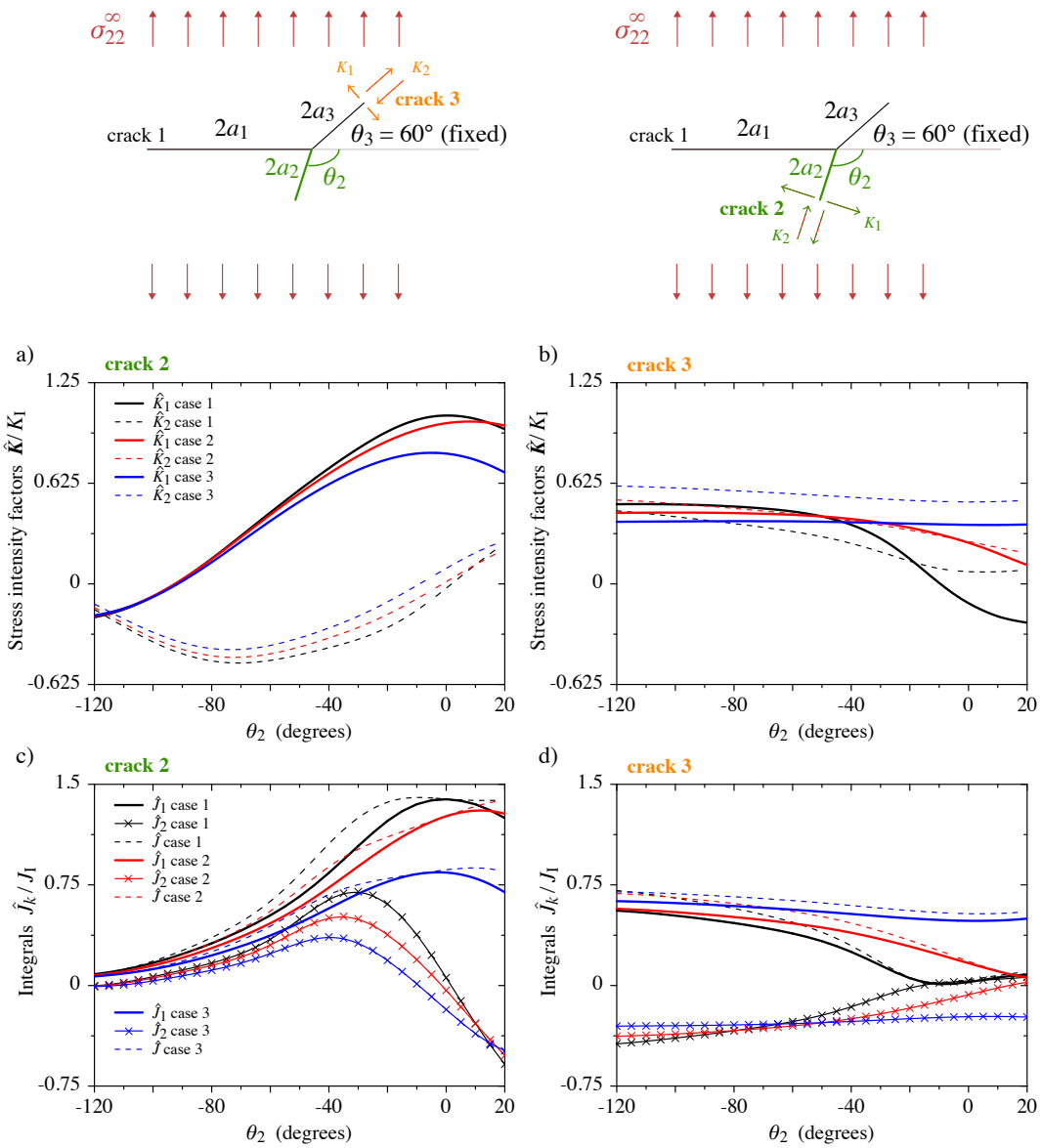

Figure 7: Variation of the stress intensity factors $\hat{\boldsymbol{K}}$ and $\hat{J}_k$-integrals for various configurations of single forked cracks. Three cases with different crack lengths are investigated, while θ_2 is the varying angle of crack 2, as pictured in the schematics.

and discussed with respect to the predictions indicated by the crack-tip $\boldsymbol{K}$-based criteria for anisotropic solids. The influence played by the short-range interactions, anisotropic elasticity, elastic mismatch, applied stress direction, inter-crack spacings and crack length ratios of various kinked and forked crack geometries are investigated in the view to revealing significant differences between both classical J_k- and $\boldsymbol{K}$- based predictions in facture mechanics.

Extensions of the present work to the fundamental case of interfacial cracks interacting with free surfaces using appropriate field solutions of intrinsic dislocation networks (Vattré, 2015, 2016) is left to follow-on analyses.

References

Amestoy, M., Leblond, J.B., 1992. Crack paths in plane situations−II. Detailed form of the expansion of the stress intensity factors. International Journal of Solids and Structures, 29, 465-501.

Asaro, R. J., Hirth, J. P., Barnett, D. M., Lothe, J., 1973. A further synthesis of sextic and integral theories for dislocations and line forces in anisotropic media. Physica Status Solidi (b), 60, 261-271.

Aubry, S., Fitzgerald, S.P., Dudarev, S.L., Cai, W., 2011. Equilibrium shape of dislocation shear loops in anisotropic α-Fe. Modelling and Simulation in Materials Science and Engineering, 19, 065006.

Azhdari, A., Nemat-Nasser, S., 1996. Energy-release rate and crack kinking in anisotropic brittle solids. Journal of the Mechanics and Physics of Solids, 44, 929-951.

Barnett, D. M., Swasger, L. A., 1971. The elastic energy of a straight dislocation in an infinite anisotropic elastic medium. Physica Status Solidi (b), 48, 419-428.

Barnett, D. M., Lothe, J., 1974. An image force theorem for dislocations in bicrystals. Journal of Physics F: Metal Physics, 4, 1618-1635.

Barr, D.T., Cleary, M.P., 1984. Thermoelastic fracture solutions using distributions of singular influence functions – Determining crack stress fields from dislocations distributions. International Journal of Solids and Structures, 19, 73-82.

Belov, A.Y., Chamrov, V.A., Indenbom, V.L., Lothe, J., 1983. Elastic fields of dislocations piercing the interface of an anisotropic bicrystal. Physica Status Solidi (b), 119, 565-578.

Bilby, B.A., Bullough, R., Smith, E., 1955. Continuous distributions of dislocations: New application of the methods of non-Riemannian geometry. Proceedings of the Royal Society of London A, 231, 263-273.

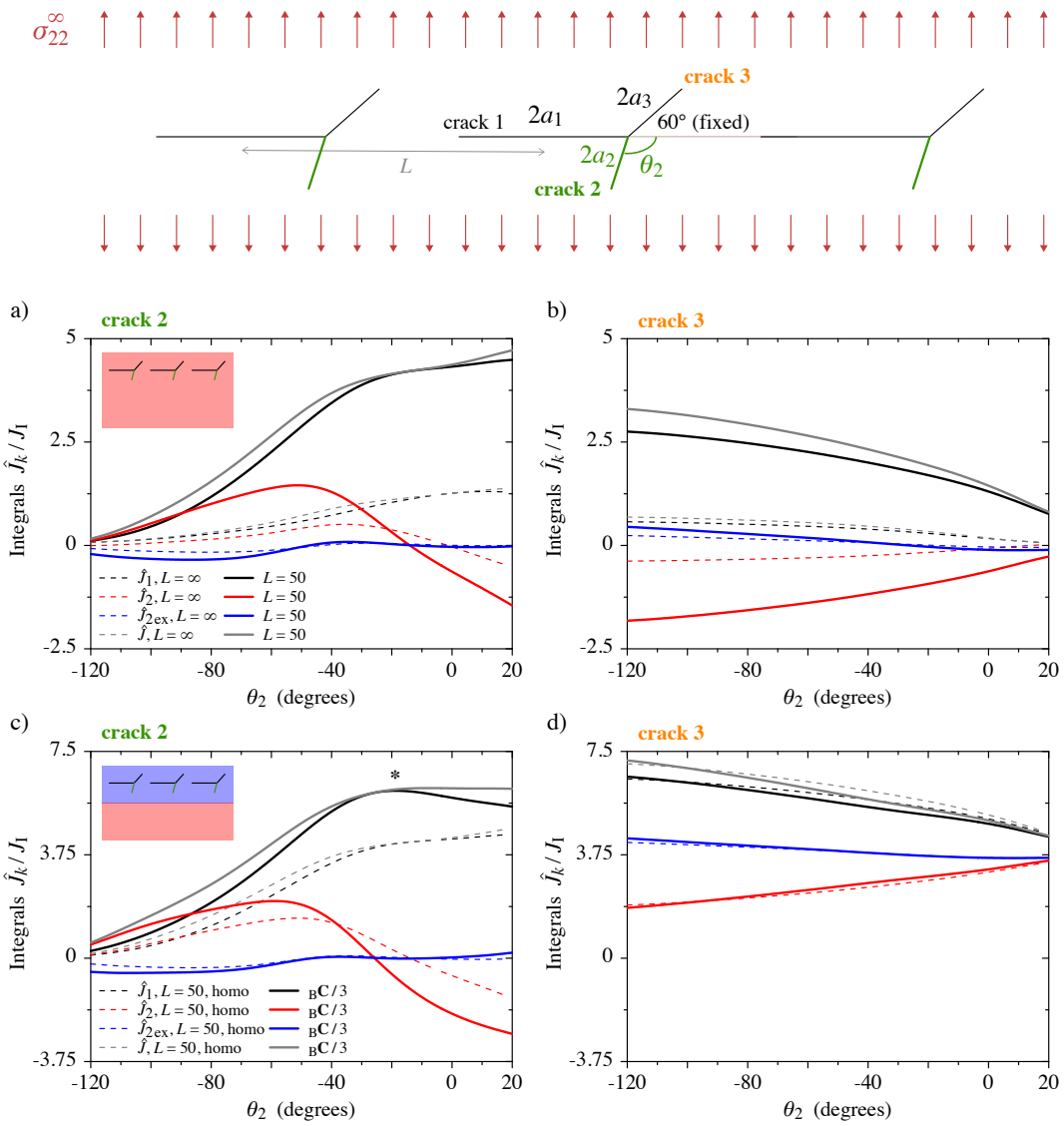

Figure 8: Effect of the inter-crack spacings and the elastic mismatch on the $\hat{J}_k$-integrals for the network of forked cracks.

Bilby, B. A., Eshelby, J. D., 1968. Dislocations and the Theory of Fracture. Academic Press: New York and London.

Bilby, B. A., Cardew, G. E., 1975. The crack with a kinked tip. International Journal of Fracture, 11,708-712.

Bilby, B. A., Cardew, G. E., Howard, I.C., 1977. Stress intensity factors at the tips of kinked and forked cracks. Facture 1977, 3, 197-200.

Budiansky, B., Rice, J.R., 1993. Conservation laws and energy-release rates. Journal of Applied Mechanics, 40, 201-203.

Bullough, R., Bilby, B.A., 1956. Continuous distributions of dislocations: Surface dislocations and the crystallography of martensitic transformations. Proceedings of the Royal Society of London B, 69, 1276-1286.

Chatterjee, S.N., 1975. The stress field in the neighborhood of a branched crack in an infinite elastic sheet. International Journal of Solids and Structures, 11, 521-538.

Chinnery, M.A., Petrak, J.A., 1967. The dislocation fault model with a variable discontinuity. Tectonophysics, 5, 513-529.

Chou, Y.T., Lin, L.S., 1975. Instability of edge dislocation walls in a two-phase isotropic medium. Materials Science and Engineering, 20, 19-27.

Chou, Y.T., 1975. Interaction of parallel dislocations in a hexagonal crystal. Journal of Applied Physics 33, 2747-2751.

Chou, Y.T.,, Pande, C.S., Yang, H.C., 1975. Interfacial edge dislocations and dislocation walls in anisotropic two-phase media. Journal of Applied Physics 46, 5-10.

Chu, H., Pan, E., 2014. Elastic fields due to dislocation arrays in anisotropic bimaterials. International Journal of Solids and Structures, 51, 1954-1961.

Cotterell, B., Rice, J.R., 1980. Slightly curved or kinked cracks. International Journal of Fracture, 16, 155-169.

Delameter, W.R., Herrmann, G., Barnett, D.M., 1975. Weakening of an elastic solid by a rectangular array of cracks. Journal of Applied Mechanics, 42, 74-80.

Eischen, J.W., 1987. An improved method for computing the J_2 integral. Engineering Fracture Mechanics, 26, 691-700.

Erdogan, F., Sih, G.C., 1963. On the crack extension in plates under plane loading and transverse shear. ASME Journal of Basic Engineering, 85, 519-527.

Erdogan, F, Gupta, G.D., Cook, T.S., 1973. Numerical solution of singular integral equations. Mechanics of fracture, 1, 368:425.

Eshelby, J.D., 1951. The force on an elastic singularity. Philosophical Transactions of the Royal Society of London, Series A, 244, 87-112.

Eshelby, J.D., Read, W.T., Shockley, W., 1953. Anisotropic elasticity with applications to dislocation theory. Acta Metallurgica, 1, 251-259.

Fil'shtinskii, L.A., 1974. Interaction of a doubly periodic system of rectilinear cracks in an isotropic medium. Journal of Applied Mathematics and Mechanics, 38, 853-861.

Gao, H., Chiu, C.H., 1992. Slightly curved or kinked cracks in anisotropic elastic solids. International Journal of Solids and Structures, 29, 947-972.

Goldstein, R.V., Salganik, R.L., 1974. Brittle fracture of solids with arbitrary crack. International Journal of Fracture, 10,507-523.

Gosling, T.J., Willis, J.R., 1994. The energy of arrays of dislocation in an anisotropic half-space. The Philosophical Magazine: A, 69, 65-90.

Grekov, M.A., Sergeeva, T.S., 2020. Interaction of edge dislocation array with bimaterial interface incorporating interface elasticity. International Journal of Engineering Science, 149, 103233.

Griffith, A.A., 1921. The phenomenon of rupture and flow in solid. Philosophical Transactions of the Royal Society of London, Series A, 221, 163-198

Gurtin, M.E., Podio-Guidugli, P., 1996. Configurational forces and the basic laws for crack propagation, 1996. Journal of the Mechanics and Physics of Solids,

44, 905-927.
Gutkin, M.Y., Militzer, M., Romanov, A.E., Vladimirov, M.I., 1989. Equilibrium position of misfit dislocations. Physica Status Solidi (a), 113, 337-344.
He, M.Y., Hutchinson, J.W., 1989. Kinking of a crack out of an interface. Journal of Applied Mechanics, 56, 270-278.
Hellen, T.K., Blackburn, W.S., 1975. The calculation of stress intensity factors for combined tensile and shear loading. International Journal of Fracture, 11, 605-617.
Herrmann, A.G., Herrmann, G., 1981. On energy release rates for a plane crack. Journal of Applied Mechanics, 48, 525-528
Hills, D.A., Kelly, P.A., Dai, D.N., Korsunsky, A.M., 1996. Solution of Crack Problems: The Distributed Dislocation Technique. Dordrecht: Kluwer.
Hirth, J.P., Barnett, D.M., Lothe, J., 1979. Stress fields of dislocation arrays at interfaces in bicrystals. Philosophical Magazine, 40, 39-47.
Hirth, J.P., Lothe J., 1992. Theory of Dislocations. 2nd ed. Melbourne: Kriger.
Huang, H., Kardomateas, G.A., 2001. Mixed-mode stress intensity factors for cracks located at or parallel to the interface in bimaterial half planes. International Journal of Solids and Structures, 38, 3719-3734.
Ichikawa, M., Tanaka, S., 1982. A critical analysis of the relationship between the energy release rate and the stress intensity factors for non-coplanar crack extension under combined mode loading. International journal of Fracture,18, 19-28.
Ioakimidis, N.I., Theocaris, P.S., 1978. Doubly-periodic array of cracks in an infinite isotropic medium. Journal of Elasticity, 8, 157-169.
Kachanov, M., 1987. Elastic solids with many cracks: A simple method of analysis. International Journal of Solids and Structures, 23, 23-45.
Kachanov, M., 2003. On the problems of crack interactions and crack coalescence. International Journal of Fracture, 120, 537-543.
Kelly, A., Tyson, W.R., Cottrell, A.H., Ductile and brittle crystals. The Philosophical Magazine: A, 15, 567-586.
Khrapkov, A.A., 1971. The first basic problem for a notch at the apex of an infinite wedge. International Journal of Fracture Mechanics, 7, 373-382.
Kitagawa, H., Yuuki, R., Ohira, T., 1975. Crack-Morphological Aspects in Fracture Mechanics. Engineering Fracture Mechanics, 7, 515-529.
Koiter, W.T., 1959. An infinite row of collinear cracks in an infinite elastic sheet. Ingenieur-Archiv, 28, 168-172.
Krenk, S., 1975. On the use of interpolation polynomials for solutions of singular integral equations. Quarterly of Applied Mathematics, 32, 479-484.
Lazarus, V., Prabel, B., Cambonie, T., Leblond, J.B., 2020. Mode I+III multiscale cohesive zone model with facet coarsening and overlap: Solutions and applications to facet orientation and toughening. Journal of the Mechanics and Physics of Solids, 141, 104007.
Leblond, J.B., Frelat, J., 2014. Development of fracture facets from a crack loaded in mode I+III: Solution and application of a model 2D problem. Journal of the Mechanics and Physics of Solids, 64, 133-153.
Leblond, J.B., Lazarus, V., Karma, A., 2015. Multiscale cohesive zone model for propagation of segmented crack fronts in mode I+III fracture. International Journal of Fracture, 191, 167-189.
Lee, K.Y., 1986. Contradiction of J_k integral. International Journal of Fracture 31, R53-R54.
Leguillon, D., 2002. Strength or toughness? A criterion for crack onset at a notch. European Journal of Mechanics - A/Solids, 21, 61-72.
Leguillon, D., Murer, S., 2008. Crack deflection in a biaxial stress state. International Journal of Fracture, 150, 75-90.
Lin, B., Mear, M.E., Ravi-Chandar, K., 2010. Criterion for initiation of cracks under mixed-mode I+III loading. International Journal of Fracture, 165, 175-188.
Lo, K.K., 1978. Analysis of branched cracks. Journal of Applied Mechanics, 45, 797-802.
Lubarda, V.A., 1997. Energy analysis of dislocation arrays near bimaterial interfaces. International Journal of Solids and Structures, 34, 1053-1073.
Morse, P.M., Feshbach, H., 1953. Methods of Theoretical Physics. New-York, McGraw-Hill.
Muskhelishvili, N.I., 1953. Some Basic Problems of Mathematical Theory of Elasticity. Noordhoff, Groningen, Holland.
Narendran, V.M., Cleary, M.P., 1984. Elastostatic interaction of multiple arbitrarily shaped cracks in plane inhomogeneous regions. Engineering Fracture Mechanics, 19, 481-506.
Pan, E., Chen, W., 2015. Static Green's Functions in Anisotropic Media. Cambridge: Cambridge University Press.
Panasyuk, V.V., Savruk, M.P., Datsyshyn, A.P., 1977. A general method of solution of two-dimensional problems in the theory of cracks. Engineering Fracture Mechanics, 9, 481-497.
Püschl, W., 1985. Reactions between glide dislocations and forest dislocations in anisotropic bcc metals. Physica Status Solidi (a), 90, 181-189.
Rice, J.R., 1968. A path independent integral and the approximate analysis of strain concentration by notches and cracks. Journal of Applied Mechanics, 35, 379-386.
Rice, J.R., Thomson, R., 1974. Ductile versus brittle behaviour of crystals. The Philosophical Magazine: A, 29, 73-97.
Sih, G.C., Strain-energy-density factor applied to mixed-mode crack problems. International Journal of Fracture, 10, 305-321.
Stroh, A.N., 1958. Dislocations and Cracks in Anisotropic Elasticity. Philosophical Magazine, 3, 625-646.
Stroh, A.N., 1962. Steady state problems in anisotropic elasticity. Journal of Mathematics and Physics, 41, 77-103.
Suresh, S., Shih, C.F., 1986. Plastic near-tip fields for branched cracks. International Journal of Fracture, 30, 237-259.
Ting, T.C.T., 1992. Image singularities for anisotropic elastic half-spaces and bimaterials. The Quarterly Journal of Mechanics and Applied Mathematics, 45, 119-139.
Ting, T.C.T., 1996. Anisotropic elasticity: theory and applications. New York/Oxford: Oxford University Press.
Vattré, A., Demkowicz, M.J., 2013. Determining the Burgers vectors and elastic strain energies of interface dislocation arrays using anisotropic elasticity theory. Acta Materialia, 14, 5172-5187.
Vattré, A., 2015. Mechanical interactions between semicoherent heterophase interfaces and free surfaces in crystalline bilayers. Acta Materialia 93, 46-59.
Vattré, A., 2016. Elastic interactions between interface dislocations and internal stresses in finite-thickness nanolayered materials. Acta Materialia 114, 184-197.
Vattré, A., 2017a. Elastic strain relaxation in interfacial dislocation patterns: I. A parametric energy-based framework. Journal of the Mechanics and Physics of Solids, 105, 254-282.
Vattré, A., 2017b. Elastic strain relaxation in interfacial dislocation patterns: II. From long- and short-range interactions to local reactions. Journal of the Mechanics and Physics of Solids, 105, 283-305.
Vattré, A., Pan, E., 2018. Three-dimensional interaction and movements of various dislocations in anisotropic bicrystals with semicoherent interfaces. Journal of the Mechanics and Physics of Solids, 116, 185-216.
Volterra, V., 1907. Sur l'équilibre des corps élastiques multiplement connexes. Annales scientifiques de l'École Normale Supérieure, 24, 401-517.
Weertman, J., 1964. Continuum distribution of dislocations on faults with finite friction. Bulletin of the Seismological Society of America, 54, 1035-1058.
Wu, C.H., 1978. Maximum-energy-release-rate criterion applied to a tension-compression specimen with crack. Journal of Elasticity, 8, 235-257.
Yang S., Yang, F.G., 2000. Kinked crack in anisotropic bodies. International Journal of Solids and Structures, 37, 6635-6681.

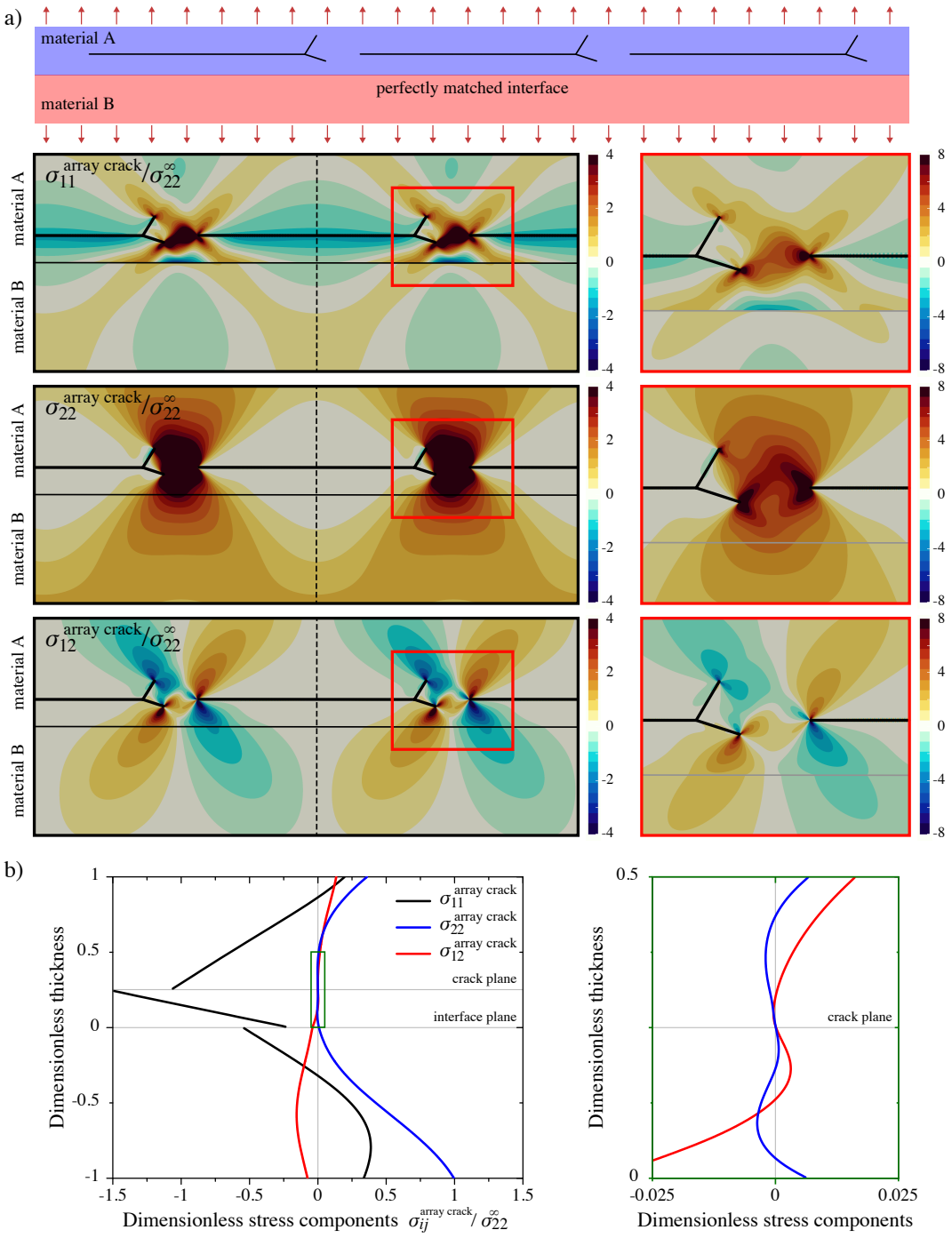

Figure 9: Dimensionless stress field solutions produced by a network of equally- and closely- spaced forked cracks in an anisotropic bimaterial under traction that corresponds to the particular configuration $*$ in Fig. (8c). (a) Contours of non-zero and dimensionless stress components. (b) Stress profiles along the vertical $\boldsymbol{x}_2$-axis, as depicted by the dotted lines in (a). The traction-free conditions on the crack planes are also satisfied.